

# Quartz fabrics in the Alpine Fault mylonites: Influence of pre-existing preferred orientations on fabric development during progressive uplift

Virginia G. Toy <sup>a,\*</sup>, David J. Prior <sup>b</sup>, Richard J. Norris <sup>a</sup>

<sup>a</sup> *Geology Department, University of Otago, P.O. Box 56, Dunedin 9054, New Zealand*

<sup>b</sup> *Earth and Ocean Sciences, University of Liverpool, 4 Brownlow Street, Liverpool L69 3GP, UK*

Received 25 May 2007; received in revised form 12 December 2007; accepted 2 January 2008

Available online 9 January 2008

## Abstract

Strong quartz crystallographic preferred orientations (CPOs) were developed during dislocation creep in the mylonite zone exposed in the hanging wall of the dextral reverse Alpine Fault Zone, New Zealand. The CPOs have a consistent asymmetry indicating a high ratio of simple to pure shear strain, with a shear sense of dextral-up to the NW, consistent with the mesoscopic shear sense indicators and with slip on the active fault. There is a transition from *Y*-maxima and asymmetric single girdles in mylonites and ultramylonites within 300 m of the present fault trace, to cross-girdle fabrics in the protomylonites further from the fault. The strong *Y*-maxima or single girdle CPOs are ascribed to high ductile shear strains under amphibolite facies conditions while the cross-girdle patterns found in the protomylonites are interpreted to represent deformation under lower temperature conditions. However, the observed fabric transition cannot logically be attributed to variations in temperature during the last increment of deformation. The highly oriented *Y*-maximum fabrics formed at high temperature contain very few grains suitably oriented for basal <a> slip, so that the slip systems activated during subsequent shear at lower temperatures during exhumation were prism <a> or rhomb <a>. Further from the fault, where shear strains under high temperature conditions were lower, weaker fabrics developed under these conditions were modified at higher levels in the crust into crossed girdle patterns. This interpretation implies that intense localisation of shear strain along the fault zone within the lower crust must have occurred in order for the high-temperature fabrics to become sufficiently intense to be preserved. This in turn implies that deep-seated localised shear was taking place early during the evolution of the current oblique-slip plate boundary fault. The results of this study also indicate that the current model that operation of certain slip systems in quartz is mostly a function of temperature is incorrect. Future work should consider the effects of deformation history, total strain and the presence of other mineral phases.

© 2008 Elsevier Ltd. All rights reserved.

**Keywords:** Alpine Fault; Quartz; Crystallographic preferred orientation (CPO); Exhumation; High strain; Geometric softening

## 1. Introduction

Quartz microstructures and crystallographic preferred orientation (CPO) textures are often used to make inferences about deformation temperatures, strain state and deformation mechanisms that operated in exhumed ancient shear zones (e.g. Behrmann and Platt, 1982; Willingshofer and Neubauer, 2002; Law et al., 2004). These data are usually interpreted by comparison with the results of experimental studies (e.g. Hirth and Tullis, 1992; Heilbronner and Tullis, 2002, 2006), or with

a few natural examples where the rates and conditions under which the microstructures and textures formed are well constrained using geochronology and thermobarometry (e.g. Dunlap et al., 1997; Stipp et al., 2002b). However, kinematic boundary constraints during natural deformation must almost always be inferred from the finite strain preserved in the shear zone rocks. Deformation kinematics can be more precisely constrained in experimental studies, but these are undertaken at high temperatures and higher strain rates than are usually encountered in nature (e.g. Ralser et al., 1991), so large extrapolations must be made to relate the results to natural situations (Brodie and Rutter, 2000; Stipp et al., 2002a). Furthermore, the total strains attained in these experiments are usually

\* Corresponding author. Tel.: +64 3 479 9088; fax: +64 3 479 7527.

E-mail address: virginia@geology.co.nz (V.G. Toy).

low; simple shear strains of  $<10$  are commonly reported (e.g. Dell'Angelo and Tullis, 1989; Heilbronner and Tullis, 2002, 2006). In natural fault zones, much higher strains should be attained. For example, a simple shear strain of 100 would be accumulated in 1 million years if slip occurred at a rate of  $1 \text{ mm yr}^{-1}$  in a 10 m wide fault zone, in 2 million years for slip at  $5 \text{ mm yr}^{-1}$  in a 100 m wide zone, and in 10 million years for slip at  $10 \text{ mm yr}^{-1}$  in a 1 km wide zone. These are all reasonable rates and dimensions for natural shear zones.

CPO fabric types vary according to the dominant intracrystalline slip systems that were active during deformation (Lister and Paterson, 1979; Schmid and Casey, 1986). The traditional view has been that slip system activity is dominantly temperature-controlled (Okudaira et al., 1995; Takeshita, 1996; Kurz et al., 2002). Recent experimental results (Heilbronner and Tullis, 2006), however, illustrate a strain-induced transition between fabric types and therefore dominant slip systems, shedding doubt on this view. Unfortunately, dislocation creep of quartz cannot easily be produced in experimental apparatus at mid-crustal temperatures ( $<500 \text{ }^\circ\text{C}$ ), so it is difficult to assess the true effects of temperature variation on slip system activity from these studies and we must instead look for this information in natural shear zones.

The mylonite zone associated with the Alpine Fault, which is the main structure in the Pacific–Australian plate boundary through the South Island of New Zealand, provides an opportunity to examine structural development during variable strains, which range up to the highest simple shear strains measured to date. Deformation occurred along a retrograde P–T path, which should be a typical situation in most shear zones with a dip-slip component to motion. Shear zone boundary kinematics are well-constrained. The thrust component of slip on the Alpine Fault has caused uplift and exhumation of material in the hanging-wall; hence the rocks presently exposed at the surface were deformed under similar conditions as those inferred to be currently active in the fault zone at depth. This contribution focuses on the quartz microstructures and CPO fabrics attained during ductile deformation within the mylonite zone associated with this major fault, in order to determine how the preserved microstructures and CPOs reflect the strain kinematics and deformation processes during progressive shear zone evolution.

## 2. Geological setting of the Alpine Fault mylonite zone

### 2.1. Tectonic setting

The Alpine Fault (Fig. 1) and a narrow crustal zone adjacent to it accommodate approximately 70% of the total Pacific–Australian plate motion in the central South Island, New Zealand (Norris and Cooper, 2001). Present-day slip rates in the central portion have been estimated as  $27 \pm 5 \text{ mm yr}^{-1}$  dextral strike slip and approximately  $8\text{--}10 \text{ mm yr}^{-1}$  of reverse dip slip from offset of Late Quaternary features (Bull and Cooper, 1986; Norris and Cooper, 2001). Exhumation rates of  $6\text{--}9 \text{ mm yr}^{-1}$  are indicated by Ar/Ar and fission track dating (Tippett and Kamp, 1993; Batt and Braun, 1999; Little

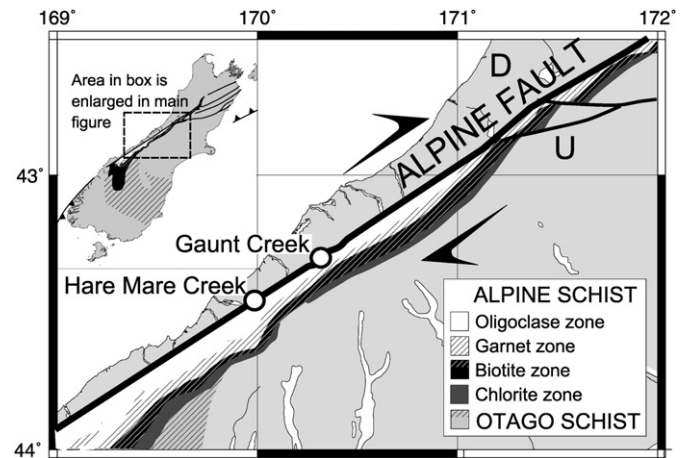


Fig. 1. Tectonic map of the South Island of New Zealand. Metamorphic grades in the Alpine schist are indicated. Locations of the two studied sections through the Alpine Fault zone are indicated. A detailed location map of Gaunt Creek is shown by Cooper and Norris (1994). A detailed location map of Hare Mare Creek is shown by Norris and Cooper (1997). The town of Franz Josef Glacier is halfway between these two locations.

et al., 2005). In surface outcrops, the brittle fault is partitioned into linked segments that dip moderately ( $30\text{--}40^\circ$ ) to the SE or are near vertical (Norris and Cooper, 1995). Surface geological data (Sibson et al., 1979) indicate the fault zone dip at depth is approximately  $45^\circ$  (the average dip of the mylonite foliation); this is consistent with recent models based on magnetotelluric, seismic and GPS data (Eberhart-Phillips, 1995; Davey et al., 1998; Beavan et al., 1999; Leitner et al., 2001).

For the last 5 million years, deformation has been localised on to a single through-going structure which is currently manifest at the surface as a thin clay gouge zone ( $<5 \text{ cm}$  wide) at the margin of a cataclasite zone ranging in thickness from 10 to 50 m. This in turn forms the base of a mylonite zone with a thickness of approximately 1 km. The mylonites pass south-eastwards into non-mylonitised amphibolite facies schists (Fig. 1).

The Alpine Fault mylonitisation affects the Alpine Schist portion of the Haast Schist. The protoliths are generally polyphase-deformed psammite and pelite (quartzo-feldspathic), with lesser volumes of metavolcanics and metachert, as well as minor meta-carbonates, although the latter are not present in either of the sections examined during this study. The quartzo-feldspathic lithology has a uniform mineralogy consisting mainly of quartz-plagioclase-muscovite-biotite  $\pm$  garnet  $\pm$  titanite  $\pm$  calcite. Variation within the quartzo-feldspathic schists is due mainly to changes in the proportions of these minerals. Metabasic lithologies mainly consist of plagioclase-hornblende-biotite  $\pm$  ilmenite  $\pm$  calcite  $\pm$  quartz  $\pm$  garnet. The metacherts are dominantly quartz with minor garnet + rutile  $\pm$  biotite  $\pm$  muscovite  $\pm$  ilmenite. The distribution of these lithologies within the Gaunt Creek and Hare Mare Creek sections are shown in Fig. 2. The Gaunt Creek section is the most complete and therefore gives the best estimate of the proportions of the various protolith lithologies; in this section metabasic mylonites outcrop for approximately 122 m of the total 1400 m covered by the cross section line

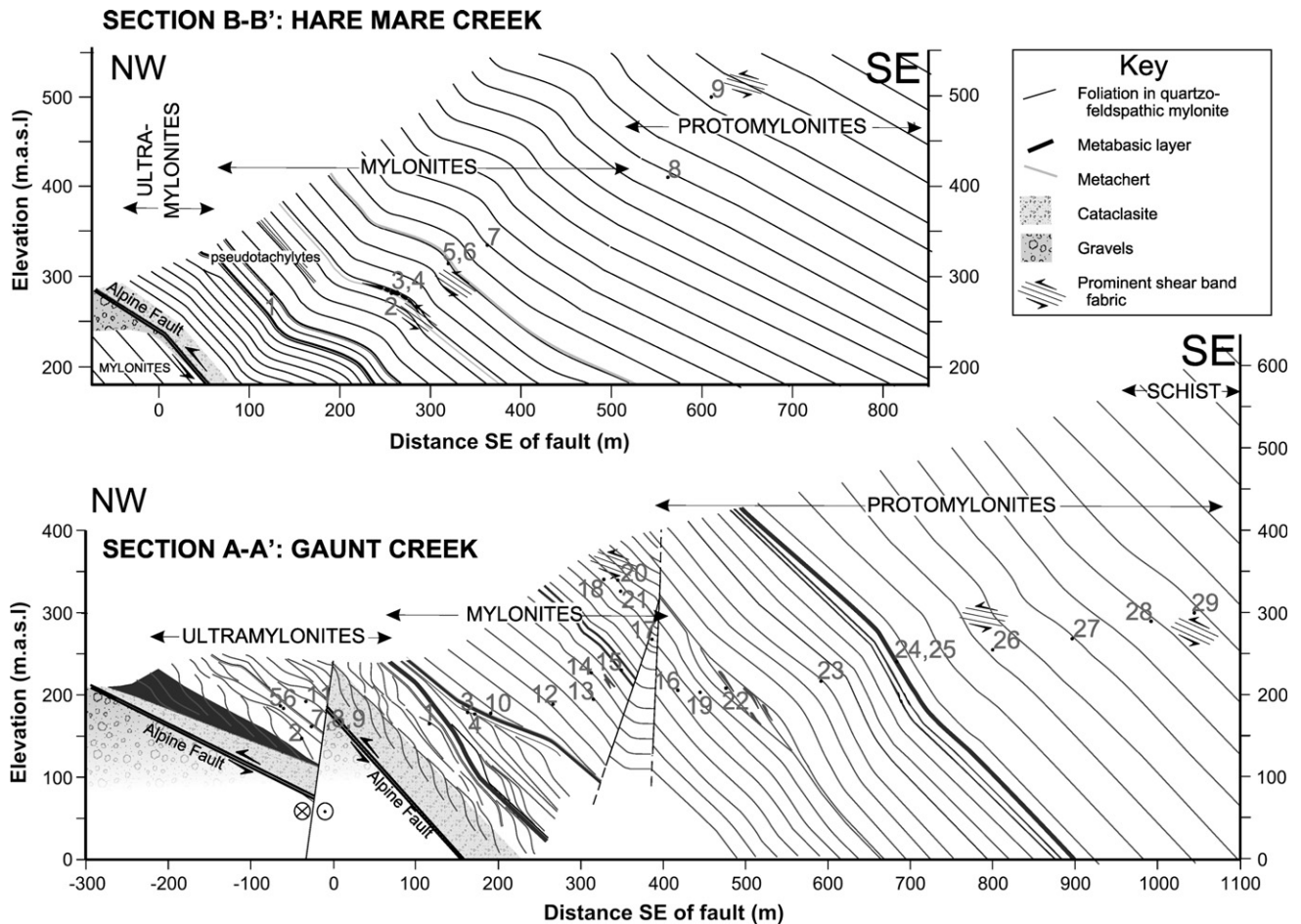


Fig. 2. Cross sections of the studied creek sections, both along bearing 125°. CPO sample locations are numbered.

(two-dimensional). This suggests that around 90% of the mylonites are quartzo-feldspathic.

Little et al. (2002a) recognised four main deformation episodes ( $D_1$  to  $D_4$ ) each producing distinct fabrics in the Alpine schists.  $D_4$  is the Cenozoic deformation related to the evolution of the present dextrally convergent plate boundary and generally strengthens the Mesozoic  $D_3$  fabrics; hence the present schist foliation is mostly  $S_{3-4}$ . This foliation is the result of distributed pure shear strain incurred during vertical thickening and rotation of the schists east of the Alpine Fault. It has been estimated that 30–40% flattening perpendicular to the foliation was accommodated during this deformation (Little et al., 2002a). The mylonitic fabric ( $S_m$ ) overprints  $S_4$  due to the increasing shear strain adjacent to the Alpine Fault.  $S_m$  in the study areas is commonly a composite S–C' (in the sense of Lister and Snoke, 1984), or extensional crenulation cleavage fabric (Blenkinsop and Treloar, 1995).

The mylonite zone rocks may be broadly classified into protomylonites, mylonites and ultramylonites. The protomylonites preserve pre-mylonitic schist structures, such as fold hinges, that are not preserved in the mylonites or ultramylonites. In the field mylonites and protomylonites are strongly layered and both have similar mica grain sizes; thin sections show

that there is a higher proportion of recrystallised quartz grains in the mylonites, so that average grain size is reduced. Ultramylonites are not layered and all phases have a finer grain size than they do in the mylonites.

Strains attained during ductile deformation have been estimated by analysis of thickness variations of a suite of Late Cretaceous pegmatite veins (Norris and Cooper, 2003). For a modelled pure shear strain,  $\alpha$ , of 1–3, where the flattening perpendicular to the fault zone is  $1/\alpha$ , simple shear strains in the protomylonites range from 12 to 32; in the mylonites from 100 to 200 and in the ultramylonites from 200 to 300 (Norris and Cooper, 2003). The shear strains are much higher than have previously been measured in simple shear zones as it is impossible to measure such high strains using more common methods of strain determination (Ramsay and Huber, 1983). However, similar simple shear strains could be expected to have accumulated during ductile deformation in many fault zones. In the Alpine Fault zone, a shear strain of 200 over a 5 million year period is equivalent to a strain rate of  $1.2 \times 10^{-12} \text{ s}^{-1}$ ; similarly a slip rate of  $23.2 \text{ mm yr}^{-1}$  (Sutherland et al., 2007) over the 1 km thick mylonite zone is equivalent to an average strain rate of  $7.4 \times 10^{-13} \text{ s}^{-1}$ . These values are at the faster end of typical geologically recognised creep strain rates (Pfiffner and Ramsay, 1982).

## 2.2. Sampling philosophy for this study

Samples for this study were collected in two transects approximately perpendicular to the mylonite zone in Gaunt Creek and Hare Mare Creek (Fig. 1). These two previously well-mapped localities (Cooper and Norris, 1994; Read, 1994; Norris and Cooper, 1997) are separated by approximately 25 km along strike of the fault and in both cases the fault is visible in outcrop so its location with respect to the exposed mylonite zone is well constrained. They are both located in the central section of the Alpine Fault where uplift rates are the most rapid and the footwall structure is simple. Norris and Cooper (1997) found that, at Hare Mare Creek, the fault is partitioned in the near surface (<2 km depth) into thrust segments linked by a vertical strike-slip fault. Samples for this study were collected from the mylonite zone adjacent to the active, southeasternmost fault strand. Further field mapping undertaken with sample collection has revealed that interaction of thrust and strike slip faults in the near surface has also caused repetition of the ultramylonite zone in the Gaunt Creek section, although on a smaller scale. Cross sections of the two mylonite zones showing these geometric relationships and sample locations are shown in Fig. 2. The Gaunt Creek section was more heavily sampled as it has better exposure of the quartz-rich layers analysed in this study, and the transect could be continued into the adjacent Alpine Schist protolith. An additional sample of Alpine Schist, from the Waiho River valley

(at the termination of the Franz Joseph Glacier, approximately 3 km to the SE of the Alpine Fault) was analysed during this study. The Waiho River valley is located approximately midway between the Gaunt and Hare Mare Creek mylonite sections.

## 3. Mylonite fabric elements and microstructures.

The fabric elements and typical microstructures observed in quartzo-feldspathic and metabasic lithologies are summarised in Table 1. Since this contribution focuses on the microstructures and textures developed in quartz-rich lithologies, we present more detailed descriptions and interpretations of quartz microstructures in the following paragraphs.

### 3.1. Protomylonites

In the protomylonites, quartz forms large (<4 mm long), highly flattened grains (axial ratios range from 1:3 to 1:10) which display patchy undulose extinction, and discrete intracrystalline bands ranging in width from 100 to 250  $\mu\text{m}$  between which there are small changes in extinction (elongate subgrains or deformation bands), or are made up of an equigranular aggregate of grains with low-angle misorientations to each other (subgrains). Boundaries between these large grains are generally interlobate. In many samples, small (<30  $\mu\text{m}$ ) grains of irregular size and with discrete grain boundaries occur adjacent to these interlobate boundaries (Fig. 3a). In more proximal

Table 1  
Summary of microstructural observations in the mylonite samples analysed during this study

	Fabric elements	Quartzo-feldspathic aggregates	Metabasites
Protomylonites	Foliation (S) is quartz-rich and mica-rich layers inherited from parent Alpine Schist C'-shear bands of Lister and Snoke (1984) or extensional crenulation cleavage ( <i>ecc</i> ; Blenkinsop and Treloar, 1995) cut S Shear band spacing 1–15 mm Shear band length <10 cm	Micas aligned with basal planes subparallel to S Shear bands (C') contain fine recrystallised green biotite, plagioclase, quartz and opaques (graphite) and some chlorite after biotite Porphyroclastic biotite 200–2000 $\mu\text{m}$ long with spiralled graphitic inclusion trails Plagioclases only altered to clay minerals around grain boundaries Garnets are microfractured and replaced by chlorite but new garnet did not form syn-mylonitically (Prior, 1993)	Hornblende and biotite grains, microfractured off larger grains are rotated into the shear bands, mostly accommodated by kinking or microfracturing parallel to (001) Retrogressive assemblage chlorite + zoisite + opaques more common than in quartzo-feldspathic materials. Often found as fine-grained aggregate in shear bands Foliation-oblique veins of calcite, chlorite and quartz are common
Mylonites and ultramylonites	Shear band fabric also present Layering becomes less distinct towards the fault (homogeneous phase distribution) Shear bands contain fine-grained biotite, plagioclase and quartz Shear band spacing $\sim$ 15 $\mu\text{m}$ Shear bands are discontinuous and anatomosing In very quartz-rich areas, slightly elongate (axial ratios $\sim$ 1:2) quartz grains define a local foliation (S) <40° oblique to mica/garnet layers which parallel the shear zone boundary (i.e. are C-planes of Lister and Snoke, 1984)	Most biotites have undergone syn-mylonitic grain size reduction Plagioclase feldspars occur as unfractured porphyroclasts composed of aggregates of slightly flattened grains or as 'fish' (cf. ten Grotenhuis et al., 2003) Plagioclase is interspersed with matrix quartz Retrogressive assemblage of sericitised plagioclase + chloritised biotite only in rare discrete layers <5 cm thick parallel to foliation Garnets strongly microfractured and often completely chloritised	Shear band fabrics (S–C' or <i>ecc</i> ) are common Retrogressive assemblages rarely developed No clear evidence for recrystallisation or neomineralisation of hornblende or lower grade equivalents such as actinolite Feldspar 'fish' are common. Most feldspars are not extensively microfractured

samples (i.e. closer to the fault), a few larger grains are found within equigranular aggregates of smaller grains that display either small changes in extinction angle with adjacent grains along straight to gently curved boundaries, or have high-angle, interlobate boundaries (Fig. 3a). The size of the grains in these aggregates is in the range 50–100  $\mu\text{m}$  and shows no systematic change with distance from the fault. The ratio of small to large grains generally increases towards the NW margin of the protomylonite zone (i.e. towards the fault). We can document a transition from large, flattened grains that are inherited from the schist protolith through to smaller recrystallised grains in the mylonites and ultramylonites.

The interlobate boundaries between these grains are evidence for strain-induced grain boundary migration recrystallisation.

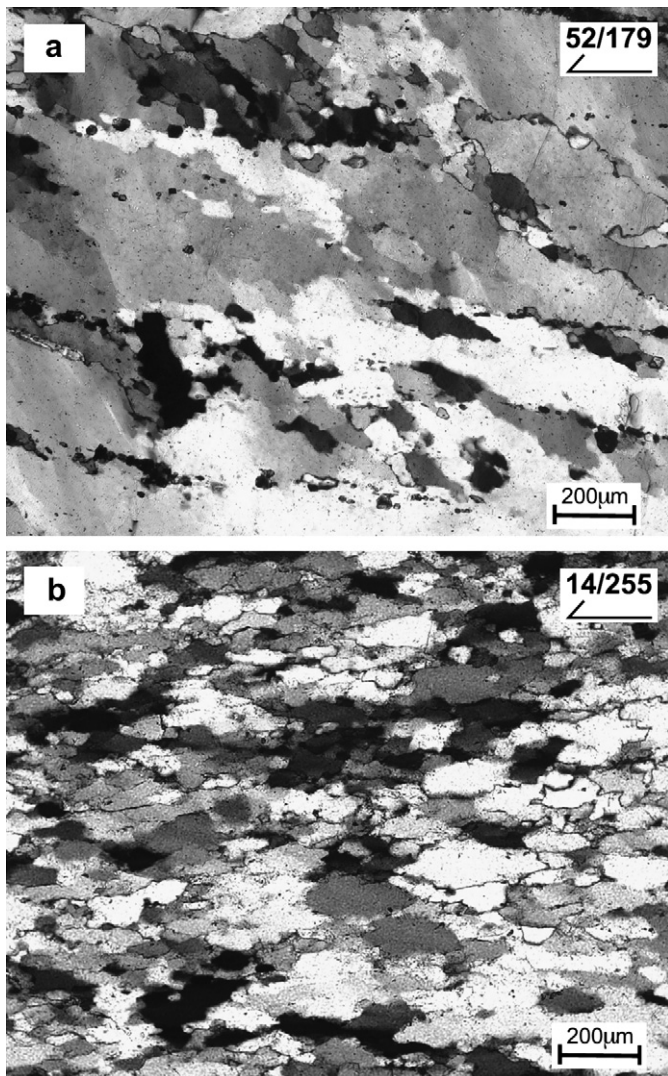


Fig. 3. Typical quartzite microstructures in (a) protomylonite (OU77931, from same position in the mylonite sequence as GC25) and (b) ultramylonite (GC8) from the Alpine Fault mylonite zone. Notice high angle grain boundaries between large remnant grains at upper right of (a). The rest of the photomicrograph area is composed of large grains with smaller, equigranular aggregates of subgrains and rarer recrystallised grains. High angle boundaries are much more common in (b) and large remnant grains with undulose extinction and deformation bands are rare.

Small, irregularly shaped grains now located near grain boundaries are interpreted as new grains formed during this process. Undulose extinction, deformation bands, and the equigranular aggregates of subgrains are evidence of recovery and may be stages in the formation of new grains by the process of subgrain rotation recrystallisation (Guillope and Poirier, 1979; White, 1976; Hirth and Tullis, 1992). These microstructures are similar to those of regimes 2 to 3 described by Hirth and Tullis (1992) in experimentally deformed quartzites.

### 3.2. Mylonites and ultramylonites

Large quartz grains with undulose extinction become much rarer in the mylonites and ultramylonites than in the protomylonites; the exceptions are less than 1000  $\mu\text{m}$  in length and decrease in size towards the fault. Most pure quartz regions consist of equigranular aggregates of slightly elongate (axial ratios <1:2) grains, ranging in size from 30  $\mu\text{m}$  to 100  $\mu\text{m}$ . There are some areas where the grains have patchy undulose extinction and display only small changes in extinction angle with the neighbouring grains. More commonly, the grain boundaries are noticeably ‘high-angle’, in which case the grains have only slight smooth undulose extinction and do not contain deformation bands, or equigranular aggregates of subgrains (Fig. 3b). Boundaries of these grains may have an interlobate shape and commonly bulge out past pinning accessory phases. Quartz microstructures within quartzo-feldspathic and metabasic mylonites are similar to those observed in pure quartz layers.

We infer that most of the remnant grains from the schist protolith have been transformed by subgrain rotation recrystallisation in these samples, forming the equigranular aggregates. Recovery to accommodate further deformation in these new grains was accommodated by grain boundary migration forming interlobate boundaries and allowing grains to grow in size slightly. These microstructures are characteristic of the regime 2/3 transition or lower regime 3 in experimentally deformed quartzites of Hirth and Tullis (1992).

A quartz microstructure that is typically observed in layers that also contain other minerals, in this case micas, is illustrated in Fig. 4a. The micas are aligned parallel to the foliation and many quartz grain boundaries coincide with them. The quartz grains are elongate parallel to the micas (i.e. in the direction in which there are no micas on grain boundaries). In quartz with fewer micas in the same sample (Fig. 4b), the grain shapes are more irregular and grain elongation parallel to mica long axes is less pronounced. The observations suggest that the micas pin the quartz grain boundaries and force grain boundary migration to occur preferentially in the foliation-parallel direction, elongating the grains in this direction rather than at an oblique angle to foliation as is often observed in pure quartz regions.

### 4. Kinematic information in the mylonites

Lineations are commonly only weakly developed in many of the mylonites. Where present they are of four types: (1)

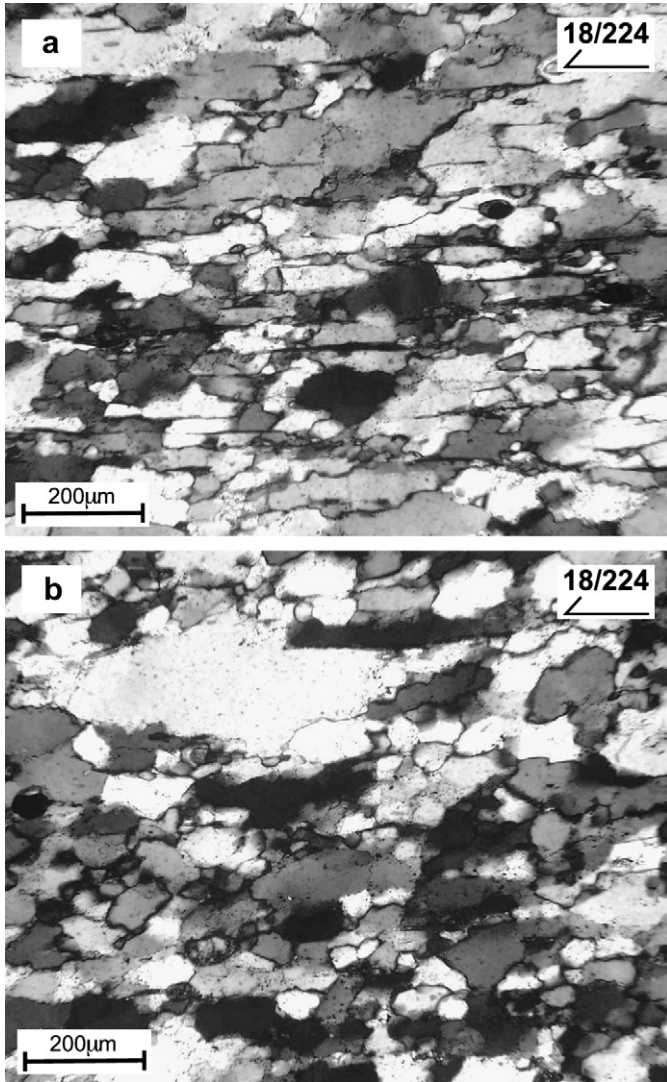


Fig. 4. These photomicrographs are both from the same sample (GC10). They illustrate the effect of the presence of a second mineral phase on the development of quartz grain shapes. (a) The presence of mica pins the quartz grain boundaries and prevents grain growth perpendicular to the foliation resulting in a rectangular aggregate of grains. (b) Pure quartz develops an inequigranular distribution of grains with interlobate boundaries.

quartz rods derived from Alpine Schist fold hinges similar to a  $D_{2(x3?)}$  quartz rodding lineation observed at Franz Joseph Glacier by Holm et al. (1989) and Little et al. (2002b), truncated by mylonitic shear bands and progressively rotated in the fault zone; (2) discontinuous streaks of biotite or other phyllosilicates on quartzose surfaces; (3) elongate, microfractured feldspar augen or ‘string-bead’ feldspar streaks on foliation surfaces; and (4) crenulations due to the intersection of shear bands and S-surfaces within the mylonites. Brittle wear striations are observed on some foliation planes (Cooper and Norris, 1994; Norris and Cooper, 1995, 1997; and authors’ own observations). The weak development of lineations is inferred to be the result of homogenisation of grain sizes during the high strains experienced by the mylonites and will be discussed further in a separate contribution.

There are a number of different microscopic shear sense indicators in the mylonites. The following shear sense indicators always show top to the N, NW or W sense of shear:

- (a) Sigma shaped objects, mostly feldspar porphyroclasts, commonly with mica tails which may originate from micaceous alteration (sericitisation) of the feldspars, indicating mild retrogressive effects (Fig. 5a).
- (b) Delta shaped objects, which are usually minerals that behave much more rigidly than quartz at the temperatures realised in the mylonite zone, such as garnet, amphibole and titanite porphyroclasts.
- (c) Mica fish (as per Lister and Snoke, 1984), usually formed of residual biotite or muscovite grains up to 1000  $\mu\text{m}$  long.
- (d) Shear band fabrics consisting of a spaced cleavage of mica-rich and quartz/feldspar-rich domains offset by localised shear bands of variable spacing depending on the mylonite grade. This is similar to a Type I S–C’ fabric

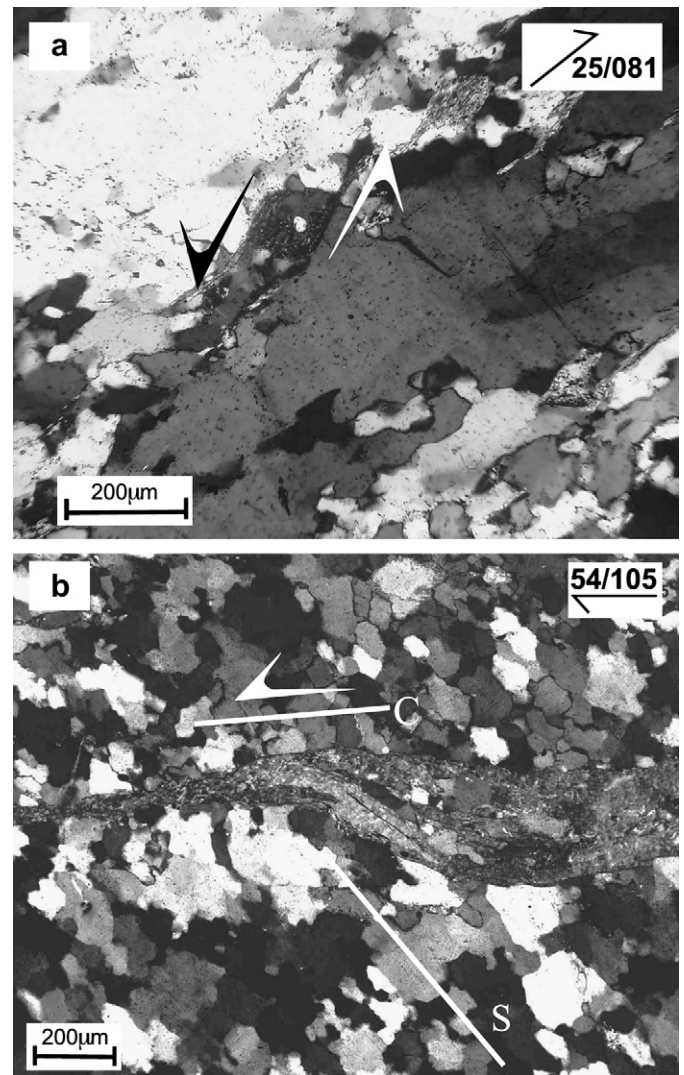


Fig. 5. Shear sense indicators in Alpine fault mylonites, both showing top to the W shear sense (a) sigma-object feldspar porphyroclast in GC27; (b) Type II S–C fabric of Lister and Snoke (1984) in GC12.

as defined by Lister and Snoke (1984) or an extensional crenulation cleavage (Blenkinsop and Treloar, 1995). Microscopic S–C fabrics similar to Type II of Lister and Snoke (1984) are in places developed in quartz-rich domains in the mylonite and ultramylonite zones (Fig. 5b).

## 5. Sample details and data collection methods for CPO fabric analyses

Crystallographic preferred orientation (CPO) data were collected from quartz-rich layers within the quartzo-feldspathic and metabasic mylonites, from pure quartz bands that may be foliation-parallel quartz veins and from metachert layers. Most of the samples analysed contain at least one secondary mineral phase. The metacherts usually contain small (<20 µm) garnets

and white micas aligned parallel to the macroscopic foliation. Quartz-rich bands in quartzo-feldspathic schist may contain from 20–50% feldspar. Sample details are summarised in Table 2.

CPO analyses were performed with a CamScan X500 Scanning Electron Microscope at the University of Liverpool. This SEM is equipped with a phosphor screen to detect backscattered electrons (EBSD), which are automatically indexed to determine crystal orientations using Channel5 software from HKLTechnology. A general description of this method is provided by Prior et al. (1999).

Crystallographic orientation data for this study were collected using a relatively large step size of ≤20 µm in order to sample as many different grains as possible during the available sampling time. Patterns were collected relatively slowly, to maximise quality, and indexed so that only limited (<<1%)

Table 2  
Sample details

Sample No.	Lithology	Distance from Alpine Fault <sup>a</sup> (m)	% quartz	Other minerals present
GC1	Foliation parallel quartz vein in quartzo-feldspathic ultramylonite	83	99	Opaques
GC2	Quartz-rich layer in quartzo-feldspathic ultramylonite	118	80	Feldspar, mica, opaques
GC3	Quartzo-feldspathic mylonite	128	60	Feldspar, mica, garnet, opaques
GC4	Metachert layer in quartzo-feldspathic mylonite	131	85	Mica, garnet, opaques
GC5	Quartz layer in metabasic and quartzo-feldspathic mylonite	131	>60	Feldspar, mica
GC6	Metachert layer in metabasic ultramylonite	133	80	Mica, garnet
GC7	Metachert layer in quartzo-feldspathic ultramylonite	137	>80	Mica, garnet
GC8	Foliation parallel quartz vein in metabasic ultramylonite	137	100	
GC9	Foliation parallel quartz vein in metabasic ultramylonite	137	99	Opaques
GC10	Metachert in metabasic mylonite	149	80–95	Mica, garnet
GC11	Foliation parallel quartz vein in augen metabasic ultramylonite	159	90–95	Mica, carbonate
GC12	Quartz band in quartzo-feldspathic mylonite	246	45	Feldspar, mica
GC13	Quartz band in quartzo-feldspathic mylonite	246	90	Feldspar, mica
GC14	Quartz band in metabasic mylonite	262	100	
GC15	Spessartine metachert in metabasic mylonite	293	>85	Mica, garnet
GC16	Metachert and quartzo-feldspathic mylonite	330	45	Feldspar, mica, garnet
GC17	Metachert mylonite	348	<90	Mica, garnet
GC18	Quartzo-feldspathic mylonite	351	45	Feldspar, mica
GC19	Metachert and quartzo-feldspathic mylonite	351	60–90	Feldspar, mica
GC21	Quartzo-feldspathic mylonite	356	85	Feldspar, mica, opaques
GC20	Quartzo-feldspathic protomylonite	360	>75	Feldspar, mica, garnet, opaques
GC22	Quartzo-feldspathic protomylonite	387	30	Feldspar, mica, opaques
GC23	Metachert protomylonite	461	60–70	Mica, garnet
GC24	Metachert protomylonite	541	80	Mica, garnet
GC25	Metachert protomylonite	541	85	Mica, garnet
GC26	Quartzo-feldspathic protomylonite	659	35	Feldspar, mica, garnet, opaques
GC27	Quartzo-feldspathic protomylonite	740	10–80	Feldspar, mica, garnet
GC28	Quartzo-feldspathic protomylonite	822	50	Feldspar, mica, opaques
GC29	Quartzo-feldspathic protomylonite	869	45	Feldspar, mica, garnet
GC32	Quartzo-feldspathic schist	881	>90	Feldspar, mica
GC31	Metachert, schist	881	70	Feldspar, mica
GC30	Quartzo-feldspathic schist	1090	50–60	Feldspar, mica
HM1	Metachert mylonite	239	>85	Feldspar, mica, garnet
HM2	Metachert mylonite	258	80–90	Mica, garnet
HM3	Quartzo-feldspathic mylonite	267	>95	Opaques
HM4	Quartzo-feldspathic mylonite	267	85–100	Feldspar
HM5	Metachert mylonite	268	80–90	Feldspar, mica, garnet
HM6	Metachert mylonite	268	>75	Feldspar, mica, garnet
HM7	Quartzo-feldspathic mylonite	290	>70	Feldspar, mica, opaques
HM8	Dense quartzo-feldspathic mylonite	393	45–50	Feldspar, mica, garnet, opaques
HM9	Quartzo-feldspathic protomylonite	418	>98	Mica, opaques
FJ1	Quartzo-feldspathic schist	>3 km	~50	Feldspar, mica, opaques

<sup>a</sup> Measured perpendicular to the mean foliation.

amount of mis-indexing of crystal orientation could have occurred. Resultant data collection rates were 1 point every 0.4 s. Data were processed (see Bestmann and Prior, 2003) to produce an orientation data set based on one point per grain, where grains are separated by boundaries with misorientations  $\geq 10^\circ$ . Grains containing at least 2 analysis points (i.e. mostly  $\geq 40 \mu\text{m}$  in diameter) were selected for plotting on CPO figures. This sampling scheme produces data directly comparable with data collected by universal stage techniques (e.g. Law, 1987). All CPO fabric plots are presented on lower hemisphere equal area Schmidt projections.

The general weakness or absence of lineations in the mylonites makes it difficult to present some CPO data in the commonly used finite strain reference frame, where the projection plane of the stereonet is perpendicular to the foliation ( $X$ – $Y$ -plane) and parallel to the stretching lineation ( $X$ ) (Law et al., 1994; Passchier and Trouw, 1996). To overcome this difficulty and produce CPO patterns that could be compared directly to those from other studies, in the absence of a lineation a direction was arbitrarily chosen within the foliation plane as the temporary  $X$ -axis, usually close to an E–W trend.  $C$ -axis orientations derived from EBSD analysis of these thin sections were then rotated about the  $Z$ -axis (the pole to  $S_m$ ) until the resulting pole figure resembled one of the types commonly observed in quartzites. This is similar to a procedure undertaken by Klaper (1988), where rotation through an angle  $\beta$  as defined by Simpson (1980) forced the measured girdle fabrics to go through the centre of the projection diagrams. Fortunately, there is a large body of CPO data from natural and experimentally deformed quartz, and the possible CPO patterns are well known (e.g. Schmid and Casey, 1986). The resulting intersection of the foliation plane and the horizontal plane of the stereographic projection corresponds to the  $X$ -axis and therefore represents the best estimate of the finite stretching direction within that mylonite sample. Because macroscopic lineations have a variety of origins and orientations we applied the same technique to samples containing a macroscopic lineation. However, some of these samples were initially cut parallel to the macroscopic lineations which have trends ranging from E to SW. The rotation angles ( $\beta$ ) in these cases ranged up to  $30^\circ$  clockwise and  $90^\circ$  anticlockwise. The orientations of macroscopic lineations and  $X$ -axes calculated by this method are shown in Fig. 6.

## 6. Description of CPO patterns

### 6.1. Definitions

The observed  $c$ -axis distributions (Fig. 6) can be broadly classified into three main types of fabric. These are (1)  $Y$ -maxima, (2) single girdles and (3) crossed girdles. The latter are mostly Type I of Lister (1977) but in some the two limbs of the ‘circle’ about the  $Z$ -axis flatten and their intersection approaches the  $Y$ -axis. This may represent a transitional stage between the Type I and Type II crossed girdle fabrics described by Lister (1977). The symmetry of CPOs is important in their interpretation (Wenk and Christie, 1991), particularly in quartz

(Law et al., 1990). CPOs that approximate an orthorhombic symmetry, where the principal directions correspond to the  $X$  (lineation),  $Y$  and  $Z$  (pole to foliation) geometric directions of the sample will be referred to as symmetric. CPOs that approximate a monoclinic symmetry, so that the  $Y$ – $Z$  plane is not a mirror plane, will be referred to as asymmetric. The sense of asymmetry will be described as either clockwise or anti-clockwise; corresponding to the sense of the smallest rotation (around the  $Y$  direction) of fabric elements away from symmetry. In this paper clockwise and anti-clockwise refer to rotation senses as seen looking up and  $\sim$  northwest in the foliation plane.

### 6.2. Gaunt Creek

In general,  $Y$ -axis maximum fabrics are observed in pure quartz layers up to approximately 300 m from the Alpine Fault (patterns GC1, GC6, GC8, GC14; Fig. 6). These layers may be foliation-parallel (probably pre-mylonitisation) veins, or pure metacherts. In rare samples, lesser concentrations of  $c$ -axes are observed close to the  $Z$ -axis (e.g. pattern GC14). The patterns usually show anticlockwise asymmetry.

Single girdle fabrics are observed in both mono- and poly-mineralic samples from within 300 m of the fault (patterns GC2, GC3, GC4, GC5, GC7, GC8, GC9, GC10, GC12, GC13, GC15). These fabrics are always asymmetric; the girdle is rotated anticlockwise with respect to the  $X$ – $Z$ -plane.

A transition to crossed girdle fabrics occurs rapidly between 293 and 330 m from the Alpine Fault perpendicular to the foliation. However, this fabric transition occurs much closer to the fault in the case of a pure quartz vein within a metabasite (pattern GC11). Type I crossed girdle fabrics occur from this transition up to approximately 850 m from the Alpine Fault perpendicular to the foliation, although some fabrics in this zone are Type II crossed girdles (patterns GC16, GC18, GC20, GC27). The most distant mylonite sample from the fault (pattern GC29) has a fabric resembling two small circles about the  $Z$ -axis, although there are concentrations of axes within these circles. Many crossed girdle patterns are asymmetric (e.g. patterns GC16 and GC19), while others are more symmetric (e.g. pattern GC23). The degree of asymmetry of the patterns becomes less with distance from the fault within the protomylonite zone.

Fabrics in samples collected outside the mylonite zone, in the adjacent Alpine Schist, are more symmetric than mylonite fabrics. They are composed of small circles about  $Z$  (pattern GC31), a symmetric single girdle (pattern GC30), and a transitional pattern between these two types (pattern GC32).

While the three fabric types introduced above suffice to broadly describe the observed  $c$ -axis distributions, the data from this study do deviate from these ideal patterns. The  $c$ -axis maxima in the protomylonites are also asymmetrically distributed about the  $X$ – $Y$  plane, occurring mostly in the  $-Z$  region of the CPO figures. The angle between the  $Y$ -axis and the  $c$ -axis maxima in the protomylonites varies between  $20^\circ$  (possibly less as small variations were not measured as they are within measurement error) and  $58^\circ$ , averaging  $42^\circ$ .

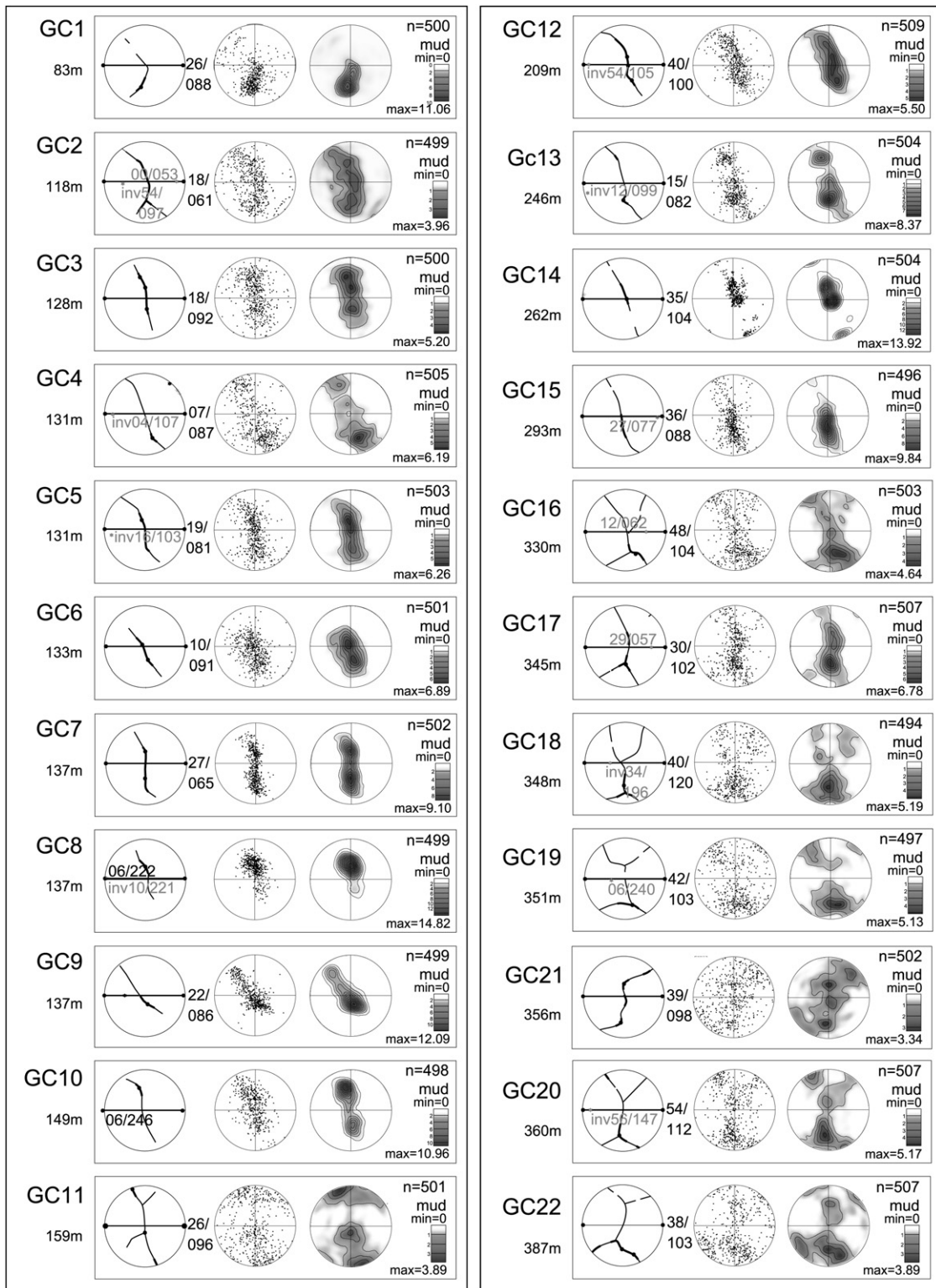


Fig. 6. Quartz CPO fabrics from Gaunt and Hare Mare Creeks. Columns, from left to right, are: sample number and distance from the Alpine Fault, finite strain reference frame and lineation information and fabric skeleton constructed from contoured c-axis plot, lower hemisphere point plot of 500 c-axes, contoured lower hemisphere equal area plot of the 500 c-axes. Stereonets are lower hemisphere Schmidt projections. The c-axis plot view is up-foliation and towards the NW. The point at right on the primitive circle of the finite strain reference frame stereonet is the X-axis of the pole figure as explained in the text. Orientations in grey on these diagrams are lineations visible macroscopically. mud = multiples of uniform density. Distances from the Alpine Fault are measured perpendicular to the average foliation (i.e. correspond to thickness measurements through the mylonite zone).

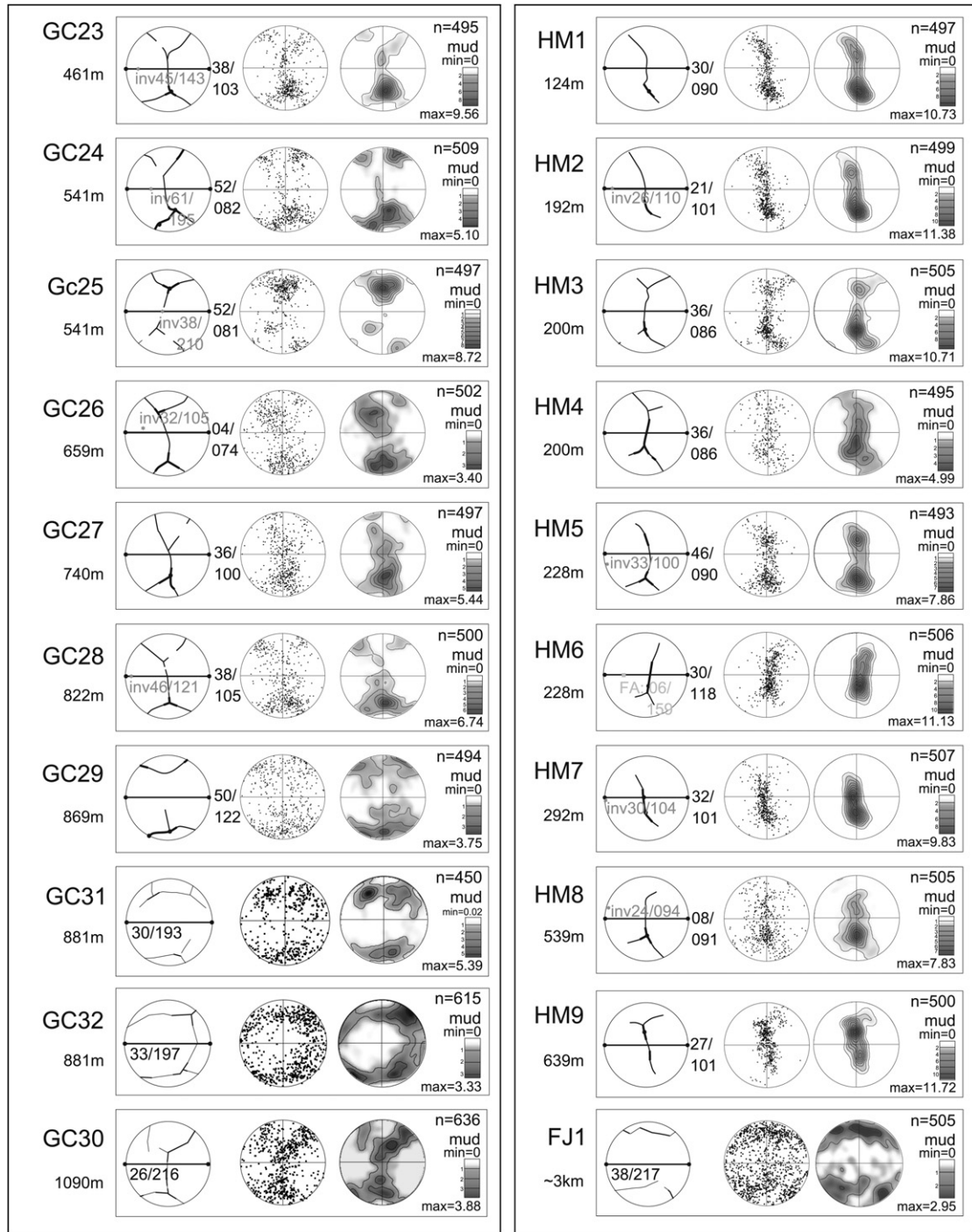


Fig. 6. (continued).

### 6.3. Hare Mare Creek

CPO patterns from samples closest to the fault are single girdles (patterns HM1, HM2; Fig. 6). Patterns HM3, HM4, HM5, HM6, HM8, and HM9 are considered to represent a transitional type between single and crossed girdles. Pattern HM7 is transitional from a Y-axis maximum to single girdle pattern. Most fabrics are rotated anticlockwise from the Y–Z plane in the sample; the exceptions being pattern HM6, where clockwise

rotation is observed and pattern HM3, which is more-or-less symmetric.

The transition from single to crossed girdle type fabric occurs in Hare Mare Creek as in Gaunt Creek, between 200 m and 300 m perpendicular to foliation from the Alpine Fault. However, the crossed girdle fabrics are not as well developed as in Gaunt Creek despite the fact that, in the Hare Mare section, there is a marked and rapid transition from mylonite to protomylonite and then to schist.

There is no obvious difference in intensity of pattern or pattern type and symmetry between lineated and non-lineated samples, aside from pattern HM7, which is a strong single girdle to  $Y$ -axis maximum much further from the fault than other patterns of its type, and which is strongly lineated. Pattern HM6 shows the opposite asymmetry to the remainder of patterns from the fault zone.

The main  $c$ -axis peak is usually in the  $-Z$  region of the CPO figure. Unlike at Gaunt Creek, however, where this occurs mostly in the lower strain protomylonite zone, at Hare Mare Creek it is more obvious in the high strain samples closer to the fault.

#### 6.4. Waiho River

The Alpine Schist sample (FJ1; Fig. 6) has a much weaker CPO than most of the mylonites. It is composed of small circles about  $Z$  with no sense of asymmetry.

### 7. Discussion and interpretation of crystallographic fabrics

#### 7.1. Intracrystalline slip, strain symmetry and kinematics

The Alpine Fault mylonite CPO patterns measured during this study are similar in general form to the commonly observed quartz  $c$ -axis patterns described by Schmid and Casey (1986). In that contribution,  $c$ -axis maxima in various parts of the CPO figure were recognised to result from different amounts of activity on basal  $\langle a \rangle$ ,  $\pm$ rhomb  $\langle a \rangle$  and prism  $\langle a \rangle$  or  $\langle c \rangle$  slip systems within a quartz crystal. The relationship between the locations of  $c$ -axis peaks on a stereographic projection and associated slip planes as indicated by Schmid and Casey's (1986) examples are summarised in Fig. 7.

All three basic CPO fabrics described above can be achieved through a combination of  $c$ -axis maxima in the various regions of Fig. 7.  $Y$ -axis maxima fabrics are a simple case of dominantly prism  $\langle a \rangle$  slip. The single girdle fabrics result from combined prism  $\langle a \rangle$  and  $\pm$ rhomb  $\langle a \rangle$  slip. In the cases where paired  $c$ -axis maxima are located between the

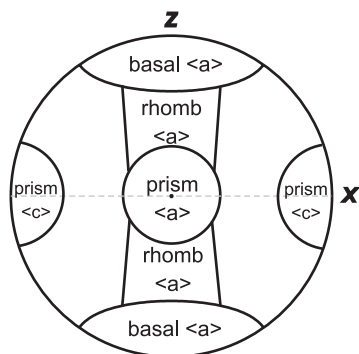


Fig. 7. Correlation between locations of  $c$ -axis peaks on CPO figures and the active slip systems in quartz. Based on Schmid and Casey (1986).  $X$  is the lineation direction,  $Z$  the pole to foliation.

$Y$ - and  $Z$ -axes,  $\pm$ rhomb  $\langle a \rangle$  slip dominates. Type I crossed girdle fabrics result from a combination of basal  $\langle a \rangle$  and prism  $\langle a \rangle$  slip; the density of points within the small circle about the  $Z$ -axis increases with increasing dominance of grains exhibiting basal  $\langle a \rangle$  slip. Type II crossed girdle fabrics occur during activity of the same slip systems if there is a departure from plane strain ( $k = 1$ ) towards constrictional strain ( $k \rightarrow \infty$ ) (Schmid and Casey, 1986).

Asymmetric single girdle  $c$ -axis fabrics in quartz were predicted by Etchecopar (1977) in models of two-dimensional simple shear deformation. The Taylor–Bishop–Hill analysis of Lister et al. (1978) produced crossed girdle fabrics only under plane strain conditions ( $k$ -values of approximately 1), whereas small circle girdles around the  $Z$ -axis were produced for flattening ( $k < 1$ ) deformation. The predominance of asymmetric single girdle or crossed girdle fabrics in the Alpine Fault mylonites therefore strongly suggests a high ratio of simple: pure shear strain. The more symmetric crossed girdle fabrics observed in the more distal protomylonites may indicate that the simple: pure shear strain ratio undergoes reduction with distance from the fault.

A fabric consisting of small circles around  $Z$  is observed in pattern GC29, the most distant sample from the Alpine Fault in the Gaunt Creek mylonite section, and in two of the samples from the Alpine Schist (GC31 and FJ1). Similar fabrics have previously been observed when pure flattening deformation ( $k = 0$ ) could be proven by independent constraints (e.g. Price, 1985; Fig. 6g). This result indicates that the flattening component of the strain is more significant in the outer parts of the fault zone and in the adjacent schists, and may explain observations of conjugate  $C'$ -shears in this region made by other authors (e.g. Holm et al., 1989; Little et al., 2002b). Much of the GC29 mylonite sample consists of high aspect ratio quartz grains with only rare recrystallised grains. The flattening component of the strain evident in the CPO pattern is most likely to be derived from these remnant grains, which indicates they experienced mostly the pure shear component of the deformation. The simple shear strain within this sample must have been accommodated mostly in shear bands and recrystallised grains. Similar microscopic-scale strain partitioning was observed in an S–C mylonite from central Australia (Kirschner and Teysier, 1991) where lozenges of elongated remnant grains were found to preserve mostly flattening strain, while higher strains with a greater rotational component were observed in the shear bands within the same sample. The crossed girdle fabrics within Alpine Fault mylonite samples that have a high fraction of recrystallised grains are inferred to dominate any contribution from the few remnant grains.

#### 7.2. Interpretation of shear sense from CPO patterns

The extraction of shear sense from CPO fabrics is based on the interpretation of fabric asymmetry (e.g. Schmid and Casey, 1986; Law et al., 1990). Schmid and Casey (1986) observed deflection of the ends of single-girdle fabrics in quartz, away from the  $Y$ – $Z$  plane and towards the direction of shear in simple shear strain histories.  $Y$ -axis maxima to single girdle

patterns produced experimentally (Heilbronner and Tullis, 2006) show a similar sense of asymmetry that is well correlated to the finite strain reference frame.

Asymmetry in Type I crossed girdle fabrics has been observed in samples deformed by simple shear (Schmid and Casey, 1986). Stronger concentrations of c-axes are expected within the limbs of the crossed girdle perpendicular to the shear plane (Lister and Price, 1978). This means that the strongest limb of the girdle is the one rotated from the  $Y$ – $Z$  plane in the direction of shear. A single girdle is equivalent to this strong limb and will also therefore be rotated from the  $Y$ – $Z$  plane. The relationship between the shear plane inferred from this geometry and the macroscopic foliation ( $X$ – $Y$ ) defines an S–C relationship from which sense of shear may be inferred.

In the Alpine Fault samples, by correlation, the observed anticlockwise rotation of all single girdles in the c-axis plots (Fig. 6) indicates a shear direction in geographic space of top to the NW, and dextral, which is consistent with the overall displacement sense of the Alpine Fault. The  $Y$ -axis maxima patterns we observe are all distributed to some degree towards the  $Z$  axis from the  $X$ – $Y$  plane similar to Heilbronner and Tullis (2006), hence the anti-clockwise rotation of these fabric elements can be used to infer the same shear sense as for the single girdles. The observed stronger anticlockwise rotated limb of the crossed girdle fabrics also indicates a dextral, top to the NW shear sense. This observation strengthens the argument that these mylonites are indeed formed during geologically recent crystal-plastic shear within the Alpine Fault zone.

### 7.3. Fabric transitions

In both mylonite sections we observe a transition from  $Y$ -maxima and single girdle fabrics to crossed girdles across the mylonite zone. This transition in fabric type approximately corresponds to the transition from mylonite to protomylonite. In the following sections we consider various factors that may have influenced this fabric transition.

#### 7.3.1. Strain dependence of fabric transitions

A transition from symmetric to progressively more asymmetric Type I crossed girdles and then to single girdles was found to occur with increasing strain during simple shear or with an increasing component of internal rotation (i.e. simple shear strain) added to a pure shear strain (Schmid and Casey, 1986). Krohe (1990) recognised variation between asymmetric crossed and single girdle fabrics as resulting only from variation in the amount of strain in shear band and lozenge domains in an S–C' mylonite. Heilbronner and Tullis (2006) observed a similar transition in experimental samples deformed to moderate shear strains. The ability of increasing strain to promote the fabric transition cannot be discounted in the Alpine Fault mylonites, since there is an order of magnitude increase in the finite strain accommodated in the ultramylonite zone compared with the protomylonites (Norris and Cooper, 2003).

The single girdle fabrics observed in the Alpine Fault mylonite samples, however, do not contain strong concentrations of c-axes near the  $Z$ -axis, unlike other natural and experimental examples of single girdle fabrics (Law et al., 1990). The asymmetric single girdles observed in the highest simple shear strain samples by Schmid and Casey (1986) most probably represent a crossed girdle fabric with one limb excessively strengthened due to the asymmetric nature of the strain. In this case there should be a number of c-axes near the  $Z$ -axis, and their absence suggests the Alpine Fault mylonite fabrics are not formed by a simple fabric evolution of this type, although this process may contribute. Furthermore, our own measurements of quartz grain shape fabrics show that there is no increase in ellipticity or grain elongation towards the fault from the protomylonites to ultramylonites. This indicates that the amount of strain accumulated in any grain is small and there is no major increase in total strain recorded by individual grains across the fault zone that could be correlated to the transition in fabric type. It should also be noted that the shear-strain in the protomylonites (Norris and Cooper, 2003) is higher than the shear-strains at which fabric transitions from cross-girdle to single girdle ( $\gamma \sim 5$ , Heilbronner and Tullis, 2006) or single girdle to  $Y$ -maximum ( $\gamma \sim 6$ – $8$ , Heilbronner and Tullis, 2006) have been reported.

Nonetheless, we cannot entirely discount the possibility that we are observing a natural system that shows a typical fabric evolution at high strains. However, if this is the case, the currently favoured models for the way that deformation occurs in quartz need to be substantially revised, since in this case, the main driving force for a change in slip system must be an increase in strain rather than a change in critical resolved shear stress (CRSS) as discussed in the next section.

#### 7.3.2. Temperature dependence of fabric transitions

It is difficult to constrain the deformation temperatures related to a CPO that may only record the latest increment of plastic strain. A quartz CPO should be reworked after only moderately low strains (Lister and Price, 1978; van Daalen et al., 1999; Heilbronner and Tullis, 2006) which would be exceeded many times over in the Alpine Fault mylonites. Like many published CPOs, those from the Alpine Fault mylonites were attained during uplift and exhumation; therefore the temperatures occurring in the rocks were likely to be decreasing during formation of the fabrics and in many cases may have been lower than those suggested by mineral thermobarometry. Thus published thermobarometric data for the Alpine Fault mylonites and Alpine Schists (Cooper, 1980; Grapes and Watanabe, 1992; Grapes, 1995; Vry et al., 2004) provides an absolute upper limit of deformation temperatures of 600–650 °C. Isolated patches of retrograde chlorite (after biotite) on shear-band planes and syn-shear fractures (Prior, 1988, 1993; authors' own observations) suggest that ductile deformation continued down to at least as low as the greenschist facies. However, it is not possible to relate the CPO development in a sample to specific conditions of deformation determined from the mineral assemblage. To further consider this

	350°C	400°C	450°C	500°C	550°C	600°C	650°C	700°C	Reference
	basal<a>			prism<c>					Takeshita (1996)
	basal<a>			prism<c>					Okudaira et al. (1995)
Type II crossed girdle				X-maxima (prism<c>)					Bahattacharya & Weber (2004)
	<a>			<c>					Mainprice et al. (1986)
				Y-maxima (prism<a>)					Schmid & Casey (1986)
	crossed girdles (basal<a>)								Kruhl (1998)
	girdles (basal<a>)			Y-maxima (prism<a>)					Kurz et al. (2002)

Fig. 8. Summary of the temperature ranges in which certain quartz slip systems have been found to operate or where CPO patterns characteristic of operation of certain slip systems have been measured (see Refs. Takeshita, 1996; Okudaira et al., 1995; Bahattacharya and Weber, 2004; Mainprice et al., 1986; Schmid and Casey, 1986; Kruhl, 1998 and Kurz et al., 2002).

relationship, we now review published studies on the effects of temperature on CPOs.

For the observed transition to occur between single and crossed girdle fabrics, there must be variation in the relative activity of the basal <a>,  $\pm$ rhomb <a> and prism <a> slip systems (Schmid and Casey, 1986; Price, 1985). Slip will occur on any system provided the critical resolved shear stress (CRSS) for that plane is attained during deformation. Ralser et al. (1991) summarised the variation in CRSS for the various slip systems with varying temperature. The CRSS for basal <a> slip is not strongly dependent on temperature; the CRSS for both  $\pm$ rhomb <a> and prism <a> slip however decreases as temperature increases and eventually becomes less than for basal <a> slip. Consequently, we might expect cross-girdle fabrics, which develop when basal <a> slip is easiest (Model B quartzite of Lister and Hobbs, 1980), to be less common at higher temperatures, and Y-axis maximum fabrics, which develop due to slip on prism <a>, to be more common.

In Fig. 8, we summarise published estimates of the temperatures at which transitions between CPO patterns or activity of certain slip systems have been observed. This compilation mostly serves to illustrate the poor understanding of the effect of temperature on the activity of slip systems; however, we can conclude that cross-girdle fabrics, in which basal <a> slip is significant, occur at lower temperatures than fabrics dominated by prism <a> and rhomb <a> slip. We do not record any evidence of prism <c> slip in the Alpine Fault mylonites. From the rather inconsistent data on temperatures, the single girdle and Y-maxima patterns are likely to have been produced under high greenschist to amphibolite facies conditions, perhaps 500–600 °C, and the crossed girdles at lower temperatures. We cannot therefore explain the Alpine Fault mylonite data as representing the thermal profile across a horizontal slice of crust as temperatures within the mylonites should decrease with proximity to the fault (Koons, 1987). Strain rate may also have an effect, as in most plastic deformation mechanisms, decreasing strain rates have the same effect as higher temperatures (Hirth and Tullis, 1992); however, in the case of the Alpine Fault mylonites, we can rule out a time-averaged decrease in strain rate towards the fault.

The microstructures and fabrics preserved in the ultramylonites, mylonites and protomylonites of the mylonite sequence now at the surface may not all have formed at the

same depth and the same time. Calculations of microstructural recycling rates (Prior et al., 1990) suggest that microstructures and CPOs will continue to evolve up until the transition from crystal-plastic to brittle deformation. The temperature at which this transition occurs is proportional to the strain rate. Since the Alpine Fault ultramylonites and mylonites accumulate a higher strain over the same time period as the protomylonites (Norris and Cooper, 2003), they must also experience a higher strain rate, so that they will pass through this brittle–viscous transition at a higher temperature. This could result in preservation of a higher temperature c-axis fabric.

The physical plausibility of this explanation can be assessed by estimating the difference in temperature at the brittle–viscous transition, in the ultramylonites versus the protomylonites. This can be done using simple crustal strength profiles (Fig. 9) calculated using an upper crustal Coulomb rheology and a lower crustal power law rheology for the different strain-rates. The specific rheological equations used to construct this simplified plot are described in Appendix A.

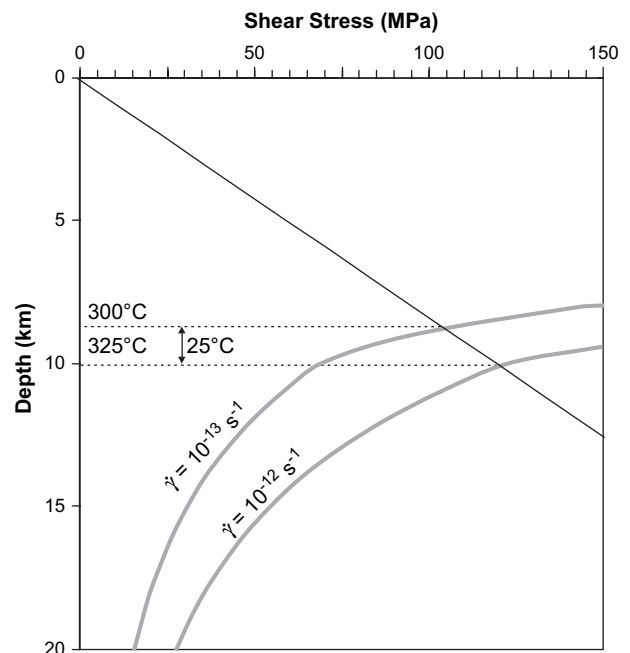


Fig. 9. Variation in the brittle–viscous transition depth due to changes in strain rate. See text for further explanation.

It is apparent from Fig. 9 that the maximum variation in temperature at the brittle-plastic transition is around 25 °C. This temperature difference is equivalent to uplift through approximately 2 km assuming a constant temperature gradient, which, at an uplift rate of 10 mm yr<sup>-1</sup> (Norris and Cooper, 2001), could occur in 0.2 million years. In this period, the total shear strain in the protomylonite zone would be of the order of 0.5–0.9. It is unlikely that this small strain would be enough to completely replace a *Y*-axis maximum fabric with the strong crossed girdle fabrics observed in the protomylonite samples.

We realise that it is possible to vary this crustal strength profile considerably by changing the input parameters. For example, if the thermal gradient is higher in the near surface, as suggested by Koons (1987), the transition from a power law to Coulomb rheology occurs at a much shallower depth. However, changing the input parameters does not significantly change the relative depths or temperatures at which the transition occurs for the protomylonite versus ultramylonite strain rates, and so does not significantly change these conclusions about the amount of additional strain accumulated during crystal-plastic deformation in the protomylonites.

### 7.3.3. Effect of inheritance on further development of CPO

From the discussions above, a purely temperature-driven transition between fabric types in the Alpine Fault mylonites seems unlikely, so that some other explanation is required. We decided to examine the effect of a pre-existing preferred orientation of quartz crystals on the development of a CPO fabric. This concept is poorly treated in the literature. Lister and Price (1978) hypothesised that further deformation under re-oriented stress axes of a material with an initial fabric could lead to one maximum of a CPO fabric being more strongly populated. Their computer model analysis, however, which dealt with the case of a decrease in strain rate or increase in temperature, the inverse of what is observed in the Alpine Fault zone, showed that the pre-existing fabric was very rapidly destroyed during further deformation. Also, in the Alpine Fault zone there is no evidence for a change in the orientation of stresses.

Ralsler et al. (1991) concluded from deformation experiments on samples that were already mylonitised that activated slip-systems were critically dependent on the orientation of pre-existing fabrics. A strongly oriented fabric formed at depth within the fault zone, at temperatures where prism <a> slip is dominant, could potentially exert a profound influence on further fabric development at lower temperatures and shallower depths where basal <a> slip becomes the preferred mechanism, since many grains would be poorly oriented for slip on the apparently 'easier' basal <a> system. Law et al. (1990) analysed relative resolved shear stresses (Schmidt factors) on various slip planes in quartz crystals for *c*-axis orientations within single girdle fabrics under simple shear. We have expanded that analysis to find relative resolved shear stresses on prism <a>, ±rhomb <a> and basal <a> slip systems for all possible orientations of the *c*-axis of a single quartz crystal in a deviatoric stress system where  $\sigma_1 = -\sigma_3$  and  $\sigma_2$  is the mean stress, that is oriented as for simple shear

as shown in Fig. 10a–c. The calculations are described in more detail in Appendix B.

We have used the results of these analyses to explore the effects of having a strong CPO on further development of that CPO. Fig. 10e shows regions where the Schmidt factors for the basal and prism slip systems exceed 0.25. Fig. 10f shows regions where the Schmidt factor for the basal slip system exceeds 0.25 and the Schmidt factor for the prism slip system exceeds 0.375. These two figures simulate decreasing activity of the prism slip relative to the basal slip, as would be expected with a decrease in temperature, from amphibolite to greenschist facies conditions (Hobbs, 1985; Takeshita, 1996). Rhomb slip would be favoured for *c*-axes in a similar orientation to those for which prism slip is favoured; we have not included rhomb slip in the analysis because rhomb slip CRSS values are generally higher than those for prism slip (Hobbs, 1985). In reality rhomb slip is probably needed to satisfy the von Mises criterion (Lister et al., 1978).

It is apparent from these analyses that for crystal orientations where the *c*-axis is located close to the *Y*-axis of the finite strain frame, slip is activated on prism <a> systems rather than basal <a> systems. If prism slip dominates in the amphibolite-facies (Fig. 10e), then we would expect *Y*-axis maxima to develop during deformation at these conditions; with the high strains experienced by the ultramylonites and mylonites, strong *Y*-axis maxima are developed, whereas in the protomylonites (that do not experience as much strain), CPOs will be much weaker. When these rocks are uplifted further into a lower temperature regime (Fig. 10f), the slip that can occur depends upon the orientations available. In the protomylonites with a weak CPO and a wide range of orientations, basal <a> slip can operate in addition to ±rhomb <a> and prism <a> slip, creating crossed girdle fabrics. In the ultramylonites and mylonites, with strong *Y*-axis maxima CPOs, slip continues to occur dominantly on prism <a> and rhomb <a> planes, strengthening the pre-existing *Y*-axis maximum fabric or forming a single girdle with the ±rhomb positions populated. The restriction to prism and rhomb slip in rocks with strong *Y*-maxima CPOs, means that these rocks may be hardened compared to rocks with different CPOs at the same temperature and strain-rate conditions. Whether this has any practical consequences in the Alpine Fault, where rocks are moving through temperature space and there are significant across strike variations in strain rate, has yet to be considered.

## 8. Implications for fault zone development

The marked asymmetry of mylonite quartz fabrics described above indicates a dominance of simple shear deformation within the fault zone. The hanging-wall schists and outer parts of the protomylonites on the other hand, exhibit more symmetrical quartz fabrics representing more co-axial strain paths. The fabrics indicate an increasing component of simple shear strain towards the present fault trace. Thus the data support the proposal that the mylonites represent a zone of highly localised intense simple shear within the lower crust. The sense of shear exhibited by the quartz fabrics is compatible

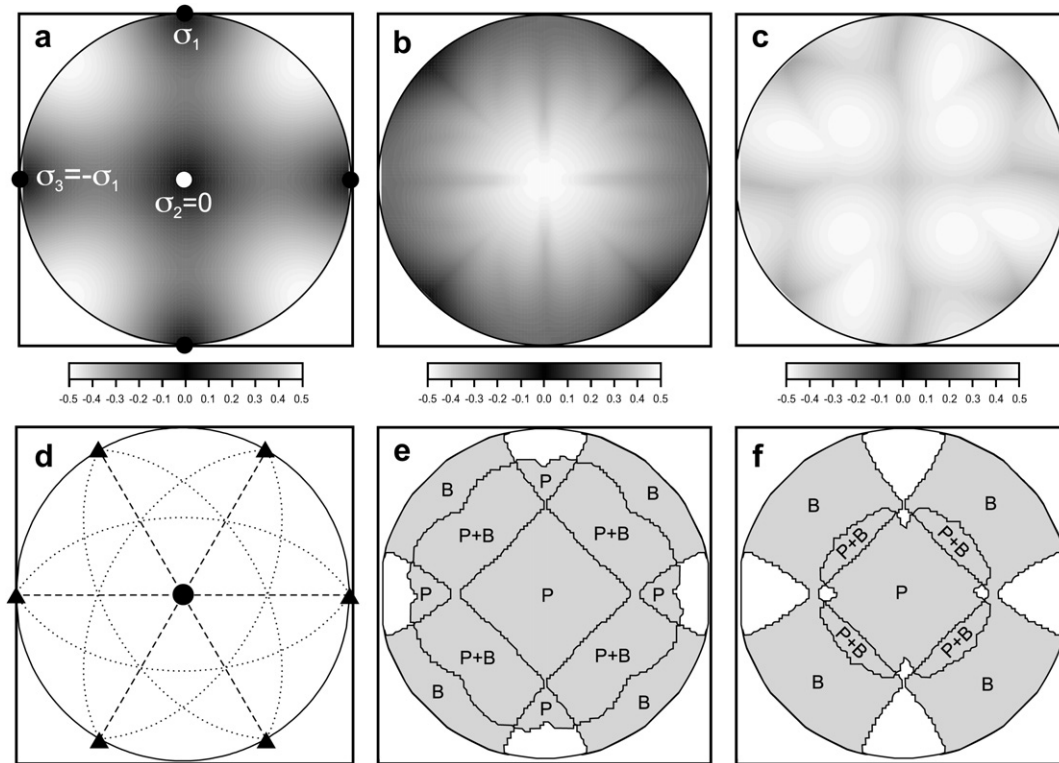


Fig. 10. Equal area stereonet contours to show the maximum Schmidt factor (normalised resolved shear stress) on specified slip planes for all possible *c*-axis orientations of a single quartz crystal. For each *c*-axis orientation, the crystal was rotated about *c* until the maximum Schmidt factor was obtained. (a) Basal  $\langle a \rangle$  slip systems. (b) Prism  $\langle a \rangle$  slip systems. (c) Positive and negative rhomb  $\langle a \rangle$  slip systems. The stress system is fixed in space as illustrated in (a) and the crystal is rotated with respect to this. A general illustration of the modelled crystal symmetry for the case where  $\varphi = 0^\circ$ ,  $\psi = 90^\circ$ ,  $\theta = 0^\circ$  is indicated in (d). Basal plane is the primitive of the stereonet; prism planes are dashed; rhomb planes are dotted; triangles are  $\langle a \rangle$ ; circle is  $\langle c \rangle$ . (e, f) Diagrams showing the region of activity of the basal  $\langle a \rangle$  and prism  $\langle a \rangle$  slip systems, for different threshold levels of the Schmidt factor corresponding to (e) amphibolite facies and (f) greenschist facies conditions. The regions of activity of rhomb slip are omitted for clarity but because of the almost uniformly high Schmidt factors, as illustrated in (c), the activity regions are only restricted if the rhomb threshold is very close to the maximum Schmidt factor. Refer to text for further discussion.

with that determined from other sense-of-shear indicators such as rotated porphyroclasts and *S*–*C/C'* structures, and with the overall sense of shear on the currently active Alpine Fault. The strain estimates reported by Norris and Cooper (2003), converted into strain rates and integrated across the mylonite zone, are also compatible with the displacement rates measured on the surface trace of the fault. Thus the kinematics of ductile strain within the mylonite zone are broadly consistent with the overall kinematics of surface faulting. This is a valuable test of the assumption that ductile deformation within deep portions of fault zones mirrors the surface displacements. Most studies of mylonite zones do not have the upper, brittle portion of the fault preserved. How ductile deformation at depth relates to near surface displacement is difficult to assess in many cases, as only either the surface fault or the mylonite zone is exposed. In most examples of the latter case, displacement has long ceased. The data presented here support the interpretation that kinematic data from mylonites may be used to infer crustal displacements, at least in some cases where the mylonites can reasonably be assumed to represent the deep portion of a major crustal fault zone (e.g. Grocott, 1977; Sibson, 1977; Berthé et al., 1979; Hanmer, 1988). It must be noted, however, that many described mylonites have relatively low strains and probably do not represent the deep

portions of plate boundary faults (e.g. Choukroune and Gapais, 1983; Bailey et al., 1994; Hanmer et al., 1995; Wenk, 1998).

The mylonites and ultramylonites developed strong *Y*-maxima or single girdle CPO patterns under amphibolite-facies conditions deep within the crust. The development of these strong fabrics representing prism  $\langle a \rangle$  and rhomb  $\langle a \rangle$  slip, would have led to geometric softening of the rocks (Poirier, 1980) due to the majority of crystals being optimally oriented for slip on the most favoured system. During exhumation, basal  $\langle a \rangle$  slip is likely to become the more favoured system, but the inherited strong high-temperature fabrics mean that prism  $\langle a \rangle$  slip is likely to continue in these strongly oriented rocks. The fact that at lower temperature, basal  $\langle a \rangle$  slip is likely to have a lower critical resolved shear stress (CRSS) than either prism  $\langle a \rangle$  or rhomb  $\langle a \rangle$  slip may result in a degree of relative hardening of these mylonites compared with the protomylonites, and a corresponding transfer of strain into the latter. As crossed girdle fabrics imply the operation of both basal  $\langle a \rangle$  and prism  $\langle a \rangle$  slip, however, clearly stresses were high enough to activate prism  $\langle a \rangle$  slip in suitably oriented grains. Thus any hardening effect is likely to be minor.

The development of a strong CPO under high temperature amphibolite facies conditions, sufficient to influence deformation at higher levels during exhumation, implies an intense

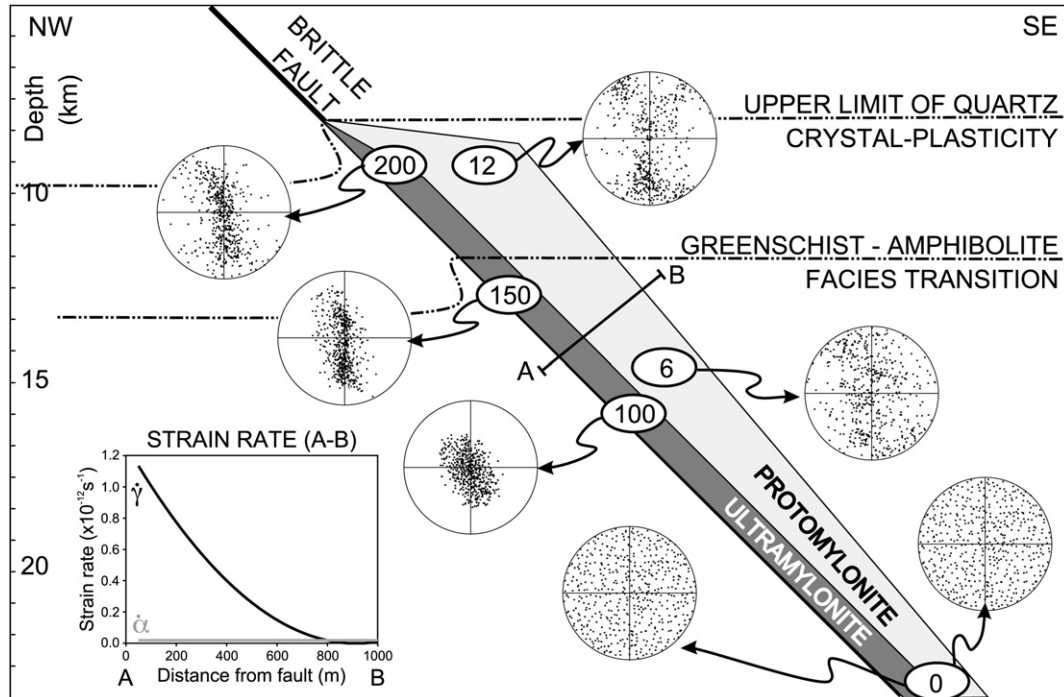


Fig. 11. Cartoon illustrating progressive development of CPOs in quartzites during deformation and exhumation in the Alpine Fault mylonite zone. Numbers in ellipses represent the total strain experienced during uplift to that level of the mylonite zone. Adjacent CPO figures are representative of the pattern that could develop with that strain amount and temperature from the starting CPO that is exhumed from deeper levels. Notice how the amount of strain at high temperatures in the protomylonites is insufficient to form a highly oriented fabric, whereas the ultramylonites exhumed through the amphibolite–greenschist facies transition already contain a strong  $Y$ -maximum pattern that is not easily destroyed during subsequent low temperature deformation. Strain rate graph is constructed using the finite strain estimates of Norris and Cooper (2003), evenly distributed over a period of 5 million years. In this cartoon the starting CPO is shown as random. In reality the Alpine schist has a weak pre-existing CPO. All areas of orientation space are represented in these weak fabrics and the pre-existing CPOs do not share the same finite strain axes as the mylonites; so for purposes of general understanding representing the pre-existing fabric as random is a reasonable simplification.

localisation of ductile strain at depths of 25 km or more below the Alpine Fault. Since at current rates of exhumation (Norris and Cooper, 2001), it would take over  $3 \times 10^6$  years for these mylonites to reach the surface, localisation must have developed at depth below the fault at an early stage of development of oblique convergence (beginning at c. 5–6 Ma; Sutherland, 1995; Walcott, 1998). This in turn suggests a greater degree of strain localisation in the underlying mantle lithosphere than has been proposed by some authors (e.g. Molnar et al., 1999) or a high degree of decoupling of lithosphere and crust (cf. Ellis et al., 2006).

## 9. Conclusions

1. The mylonites along the Alpine Fault show strong quartz CPOs, with a transition from  $Y$ -maxima and asymmetric single girdles within 300 m of the present fault trace, to cross-girdle fabrics in the protomylonites further from the fault.
2. The strong and consistent asymmetry displayed by nearly all the CPOs indicate a high ratio of simple shear to pure shear, with a shear sense of dextral-up to the NW. This is consistent with the mesoscopic shear sense indicators and with the overall slip on the active fault.
3. The strong  $Y$ -maxima or single girdle CPOs developed within 300 m of the fault trace are ascribed to high ductile shear strains at temperatures under which prism  $\langle a \rangle$  and

rhomb  $\langle a \rangle$  slip systems are dominant, i.e. under amphibolite facies conditions at depth within the lower crust.

4. The cross-girdle patterns found in the protomylonites are interpreted to represent deformation under lower temperature conditions where basal  $\langle a \rangle$  slip is dominant.
5. In this case the activity of the various slip systems, and hence the CPO pattern, does not reflect a change in temperatures experienced during the final stages of deformation, as would be a common interpretation.
6. As illustrated in Fig. 11, the transition between the two types of CPO patterns is interpreted to be mostly due to preservation of the high temperature fabric within the mylonites and ultramylonites due to its intense  $Y$ -maximum meaning there were very few grains suitably oriented for basal  $\langle a \rangle$  slip, so that the first slip system to be activated during shear would remain the prism  $\langle a \rangle$  system. Further from the fault, where the shear strains accommodated at high temperature conditions were less, weaker fabrics developed under these conditions were able to be modified at higher levels in the crust into crossed girdle patterns.
7. The observed fabric transition therefore represents different degrees of preservation of high temperature CPOs during later deformation rather than a temperature gradient during a single stage of deformation.
8. A further implication of this conclusion is that intense localisation of shear strain must have occurred along the

fault zone within the lower crust in order for the fabrics to become sufficiently intense to be preserved. This in turn implies that deep-seated localised shear was taking place early during the evolution of the current oblique-slip plate boundary fault.

## Acknowledgements

This research was supported by a University of Otago Research Grant and by the Public Good Science Fund of New Zealand (GNS FRST subcontract from C05X0402) and forms part of the first author's PhD thesis research which was carried out under a University of Otago Postgraduate Scholarship. SEM work was funded through NERC grant NER/A/S2001/01181. We are indebted to all the members of the Microstructure Research Group at the University of Liverpool for their technical advice and assistance, and to Brent Pooley of the University of Otago for specimen preparation. We also thank Alan Cooper for advice and assistance in the field and for discussion of Alpine Fault problems. Many of the contour plots were generated using GMT (<http://gmt.soest.hawaii.edu/>) and shear stress modelling was implemented in Scilab ([www.scilab.org](http://www.scilab.org)). We thank the authors of both packages for making their software open source. We are appreciative of the thorough and detailed reviews by Tim Little and Joe White that helped us to considerably improve this manuscript, and for the assistance of journal editor Tom Blenkinsop.

## Appendix A

The simplified crustal strength plot (Fig. 9) was constructed assuming that:

(a) The strength of the upper crust is the yield stress for sliding along a pre-existing foliation plane oriented 055/45SE, with  $\sigma_v' = \sigma_2'$  and  $\sigma_1'$  trending 00/119° as indicated by the hanging-wall stress tensor derived by Leitner et al. (2001) from earthquake focal mechanism inversions. It is assumed that  $\sigma_2' = 1/2 (\sigma_1' + \sigma_3')$ . The coefficient of static friction,  $\mu_s$  is 0.5; fluid pressure,  $P_f$ , is assumed to be hydrostatic and the density of the crust is  $2700 \text{ kg m}^{-3}$ . Failure occurs when  $(\sigma_1 - \sigma_3) \geq 2\sigma_v'(R - 1)/(R + 1)$  (Sibson, 1974, 1998), where  $R = \sigma_1'/\sigma_3'$  is found to meet the limiting condition for frictional failure  $\tau/\sigma_n' > \mu_s$  (Collettini and Trippetta, 2007).

$$\mathbf{R} = \begin{bmatrix} \cos\phi\cos\theta - \sin\phi\sin\theta\sin\psi & \sin\phi\cos\theta + \cos\phi\sin\theta\sin\psi & -\sin\theta\cos\psi \\ -\sin\phi\cos\psi & \cos\phi\cos\psi & \sin\psi \\ \cos\phi\sin\theta + \sin\phi\cos\theta\sin\psi & \sin\phi\sin\theta - \cos\phi\cos\theta\sin\psi & \cos\theta\cos\psi \end{bmatrix} \quad (\text{A3})$$

(b) The strength of the lower crust is the flow stress for constant strain rate of a quartz aggregate deforming by dislocation creep according to the flow law of Hirth et al. (2001), adapted to simple shear using the factor  $\sqrt{(3^{n+1})}$  as per Nye (1953).

Strain rates within the mylonites are found by assuming that the total strains determined by Norris and Cooper (2003) were distributed evenly over the  $\sim 5$  million year history of mylonitic deformation, resulting in strain rates varying from  $10^{-12} \text{ s}^{-1}$  in the ultramylonites to  $10^{-13} \text{ s}^{-1}$  in the protomylonites. The temperature-depth distribution is found by assuming that a maximum temperature of c. 600 °C was attained in the schists above a basal décollement at around 35 km depth (Kleffmann et al., 1998), before they were exhumed in the fault zone (Cooper, 1980; Grapes and Watanabe, 1992; Grapes, 1995; Vry et al., 2004) and that the brittle–viscous transition occurs at approximately 8–12 km, which is the cut-off of seismicity (Eberhart-Phillips, 1995; Leitner et al., 2001). We assume there is free water present so that  $P_{\text{H}_2\text{O}} = P_{\text{rock}}$  and calculate  $f_{\text{H}_2\text{O}}$  using the Basic Water Package of the software Fluidcal (Wagner and Overhoff, 2006) which is based on the IAPWS-95 formulation for the thermodynamic properties of water (Wagner and Prub, 2002).

## Appendix B

The orientations of possible slip systems for alpha-quartz are defined by unit vectors in  $\mathbf{R}^3$ , as shown in Table A1. The maximum shear stress vector,  $\boldsymbol{\tau}_{\text{max}}$ , on the slip plane with normal vector,  $\mathbf{n}$ , is related to the stress tensor,  $\boldsymbol{\sigma}$ , by the equation (Law et al., 1990):

$$\boldsymbol{\tau}_{\text{max}} = \boldsymbol{\sigma} \cdot \mathbf{n} \quad (\text{A1})$$

and the component of this maximum shear stress vector,  $\boldsymbol{\tau}_{\text{R}}$ , resolved on the slip direction,  $\mathbf{s}$ , is:

$$\boldsymbol{\tau}_{\text{R}} = \mathbf{s} \cdot \boldsymbol{\tau}_{\text{max}} \quad (\text{A2})$$

The 'crystal' is rotated around the original  $\sigma_1$ ,  $\sigma_2$  and  $\sigma_3$  orientations by the following angles:

- $\varphi$  about the  $\sigma_1$  axis
- $\psi$  about the  $\sigma_3$  axis
- $\theta$  about the  $\sigma_2$  axis

Positive angles are clockwise about the axes when viewed towards the origin. The rotation is accomplished by multiplying the slip directions and slip-plane normal vectors by the rotation matrix ( $\mathbf{R}$ ):

For all possible c-axis orientations (all  $\psi$  and  $\theta$  angles), the maximum resolved shear stress magnitude (for all possible  $\varphi$  angles) is calculated, for each of the slip systems; basal  $\langle a \rangle$ , prism  $\langle a \rangle$  and rhomb  $\langle a \rangle$  (Table 2; Fig. 10d). Calculations

are made for  $\varphi$ ,  $\psi$  and  $\theta$  increments of  $1^\circ$  or less. The Schmidt factors (normalised, from 0 to 0.5, maximum resolved shear stresses), on each of the slip systems, as a function of c-axis orientation are shown on stereonets in Fig. 10a–c. It is assumed that one of the a-axes of the model crystal is in an optimal orientation, so the calculated Schmidt factors are the maximum possible for that crystal orientation. If the crystal is not free to rotate about its c-axis, the Schmidt factors will be lower.

The resolved stresses for basal slip are highest for c-axes in the  $\sigma_1$ – $\sigma_3$  plane, at  $45^\circ$  to  $\sigma_1$  (or  $\sigma_3$ ). The resolved stresses for both prism and rhomb slip are highest for c-axes parallel to  $\sigma_2$ .

Table A1

Orientations of slip systems in model quartz crystal in Miller space and  $\mathbf{R}^3$ 

Slip plane	Miller–Bravis index	Unit vector normal to slip plane
Basal	(0001)	(0,0,1)
Prism (m)	(01–10)	(0,–1,0)
	(–1010)	(– $\sqrt{3}$ ,1,0)
+Rhomb (r)	(1–100)	( $\sqrt{3}$ ,1,0)
	(0–111)	(0,1,tan(38))
	(10–11)	( $\sqrt{3}$ ,–1,2.tan(38))
–Rhomb (z)	(–1101)	(– $\sqrt{3}$ ,–1,2.tan(38))
	(01–11)	(0,–1,tan(38))
	(–1011)	(– $\sqrt{3}$ ,1,2.tan(38))
	(10–11)	( $\sqrt{3}$ ,1,2.tan(38))

## References

- Bahattacharya, A.R., Weber, K., 2004. Fabric development during shear deformation in the Main Central Thrust Zone, NW Himalaya, India. *Tectonophysics* 387, 23–46.
- Bailey, C.M., Simpson, C., De Paor, D.G., 1994. Volume loss and tectonic flattening strain in granitic mylonites from the Blue Ridge province, central Appalachians. *Journal of Structural Geology* 16, 1403–1416.
- Batt, G., Braun, J., 1999. The tectonic evolution of the Southern Alps, New Zealand: insights from fully thermally coupled dynamical modelling. *Geophysical Journal International* 136, 403–420.
- Beavan, J., Moore, M., Pearson, C., Henderson, M., Parsons, B., Bourne, S., England, P., Walcott, D., Blick, G., Darby, D., Hodgkinson, K., 1999. Crustal deformation during 1994–1998 due to oblique continental collision in the central Southern Alps, New Zealand, and implications for seismic potential of the Alpine Fault. *Journal of Geophysical Research* 104 (B11), 25,233–25,255.
- Behrmann, J.H., Platt, J.P., 1982. Sense of nappe emplacement from quartz c-axis fabrics; an example from the Betic Cordilleras (Spain). *Earth and Planetary Science Letters* 59, 208–215.
- Berthé, D., Choukroune, P., Jegouzo, P., 1979. Orthogneiss, mylonite and non coaxial deformation of granites: the example of the South American Shear Zone. *Journal of Structural Geology* 1 (1), 31–42.
- Bestmann, M., Prior, D.J., 2003. Intragranular dynamic recrystallization in naturally deformed calcite marble: diffusion accommodated grain boundary sliding as a result of subgrain rotation recrystallization. *Journal of Structural Geology* 25 (10), 1597–1613.
- Blenkinsop, T.G., Treloar, P.J., 1995. Geometry, classification and kinematics of S–C and S–C' fabrics in the Mushandike area, Zimbabwe. *Journal of Structural Geology* 17 (3), 397–408.
- Brodie, K.H., Rutter, E.H., 2000. Deformation mechanisms and rheology: why marble is weaker than quartzite. *Journal of the Geological Society, London* 157, 1093–1096.
- Bull, W.B., Cooper, A.F., 1986. Uplifted marine terraces along the Alpine Fault, New Zealand. *Science* 234, 1225–1228.
- Choukroune, P., Gapais, D., 1983. Strain pattern in the Aar Granite (Central Alps) orthogneiss developed by bulk inhomogeneous flattening. *Journal of Structural Geology* 5, 411–418.
- Colletini, C., Trippetta, F., 2007. A slip tendency analysis to test mechanical and structural control on aftershock rupture planes. *Earth and Planetary Science Letters* 255, 402–413.
- Cooper, A.F., 1980. Retrograde alteration of chromian kyanite in metachert and amphibolite whiteschist from the Southern Alps, New Zealand, with implications for uplift on the Alpine Fault. *Contributions to Mineralogy and Petrology* 75, 153–164.
- Cooper, A.F., Norris, R.J., 1994. Anatomy, structural evolution, and slip rate of a plate-boundary thrust: The Alpine Fault at Gaunt Creek, Westland, New Zealand. *Geological Society of America Bulletin* 106, 627–635.
- Davey, F., Henyey, T., Holbrook, W.S., Okaya, D., Stern, T.A., Melhuish, A., Henrys, S., Anderson, H., Eberhart-Phillips, D., McEvelly, T., Uhrhammer, R., Wu, F., Jiracek, G.R., Wannamaker, P.E., Caldwell, G., Christensen, N., 1998. Preliminary results from a geophysical study across a modern continent-continent collisional plate boundary—the Southern Alps, New Zealand. *Tectonophysics* 288, 221–235.
- Dell'Angelo, L.N., Tullis, J., 1989. Fabric development in experimentally deformed quartzites. *Tectonophysics* 169, 1–21.
- Dunlap, W.J., Hirth, G., Teyssier, C., 1997. Thermomechanical evolution of a ductile duplex. *Tectonics* 16, 983–1000.
- Eberhart-Phillips, D., 1995. Examination of seismicity in the central Alpine Fault region, South Island, New Zealand. *New Zealand Journal of Geology and Geophysics* 38, 571–578.
- Ellis, S., Beavan, J., Eberhart-Phillips, D., 2006. Bounds on the width of mantle lithosphere flow derived from surface geodetic measurements: application to the central Southern Alps, New Zealand. *Geophysical Journal International* 166, 403–417.
- Etchecopar, A., 1977. A plane kinematic model of progressive deformation in a polycrystalline aggregate. *Tectonophysics* 39, 121–139.
- Grapes, R., 1995. Uplift and exhumation of Alpine Schist, Southern Alps, New Zealand: thermobarometric constraints. *New Zealand Journal of Geology and Geophysics* 38, 525–533.
- Grapes, R.H., Watanabe, T., 1992. Metamorphism and uplift of Alpine Schist in the Franz Joseph-Fox Glacier area of the Southern Alps, New Zealand. *Journal of Metamorphic Geology* 10, 171–180.
- Grocott, J., 1977. The relationship between Precambrian shear belts and modern fault systems. *Journal of the Geological Society, London* 133, 257–262.
- Guillope, M., Poirier, J.P., 1979. Dynamic recrystallisation during creep of single crystalline halite: an experimental study. *Journal of Geophysical Research* 84, 5557–5567.
- Hanmer, S., 1988. Great Slave Lake Shear Zone, Canadian Shield: a reconstructed vertical profile of a crustal scale fault. *Tectonophysics* 149, 245–264.
- Hanmer, S., Williams, M., Kopf, C., 1995. Modest movements, spectacular fabrics in an intracontinental deep-crustal strike-slip fault: Striding-Athabasca mylonite zone, NW Canadian Shield. *Journal of Structural Geology* 17, 493–507.
- Heilbronner, R., Tullis, J., 2002. The effect of static annealing on microstructures and crystallographic preferred orientations of quartzites experimentally deformed in axial compression and shear. In: De Meer, S., Drury, M.R., De Bresser, J.H.P., Pennock, G.M. (Eds.), *Deformation Mechanisms, Rheology and Tectonics: Current Status and Future Perspectives*. Geological Society Special Publications, 200. Geological Society, London, pp. 191–218.
- Heilbronner, R., Tullis, J., 2006. Evolution of c-axis pole figures and grain size during dynamic recrystallization: Results from experimentally sheared quartzite. *Journal of Geophysical Research* 111 (B10202), doi:10.1029/2005JB004194.
- Hirth, G., Tullis, J., 1992. Dislocation creep regimes in quartz aggregates. *Journal of Structural Geology* 14, 145–159.
- Hirth, G., Teyssier, C., Dunlap, W., 2001. An evaluation of quartzite flow laws based on comparisons between experimentally and naturally deformed rocks. *International Journal of Earth Sciences (Geologische Rundschau)* 90, 77–87.

- Hobbs, B.E., 1985. The geological significance of microfabric analysis. In: Wenk, H.-R. (Ed.), *Preferred Orientation in Deformed Metals and Rocks: An Introduction to Modern Texture Analysis*. Academic Press, Orlando, FL, pp. 463–484.
- Holm, D.K., Norris, R.J., Craw, D., 1989. Brittle and ductile deformation in a zone of rapid uplift: Central Southern Alps, New Zealand. *Tectonics* 8, 153–168.
- Kirschner, D., Teyssier, C., 1991. Quartz c-axis fabric differences between porphyroclasts and recrystallized grains. *Journal of Structural Geology* 13 (1), 105–109.
- Klaper, E.M., 1988. Quartz c-axis fabric development and large-scale post-nappe folding (Wandfluhhorn Fold, Penninic Nappes). *Journal of Structural Geology* 10 (8), 795–802.
- Kleffmann, S., Davey, F., Melhuish, A., 1998. Crustal structure in the central South Island, New Zealand, from the Lake Pukaki Seismic Experiment. *New Zealand Journal of Geology and Geophysics* 41 (1), 39–49.
- Koons, P.O., 1987. Some thermal and mechanical consequences of rapid uplift: an example from the Southern Alps, New Zealand. *Earth and Planetary Science Letters* 86, 307–319.
- Krohe, A., 1990. Local variations in quartz [c]-axis orientations in non-coaxial regimes and their significance for the mechanics of S–C fabrics. *Journal of Structural Geology* 12 (8), 995–1004.
- Kruhl, J.H., 1998. Prism- and basal-plane parallel subgrain boundaries in quartz: a microstructural geothermobarometer: Reply. *Journal of Metamorphic Geology* 16, 142–146.
- Kurz, W., Fritz, H., Tenczer, V., Unzog, W., 2002. Tectonometamorphic evolution of the Koralm Complex (Eastern Alps): constraints from microstructures and textures of the ‘Plattengneis’ shear zone. *Journal of Structural Geology* 24, 1957–1970.
- Law, R.D., 1987. Crystallographic fabrics and deformation histories. *Journal of the Geological Society*, London 144, 675–676.
- Law, R.D., Schmid, S.M., Wheeler, J., 1990. Simple shear deformation and quartz crystallographic fabrics: a possible natural example from the Torridon area of NW Scotland. *Journal of Structural Geology* 12 (1), 29–45.
- Law, R.D., Miller, E.L., Little, T.A., Lee, J., 1994. Extensional origin of ductile fabrics in the Schist Belt, Central Brooks Range, Alaska - II. Microstructural and petrofabric evidence. *Journal of Structural Geology* 16 (7), 919–940.
- Law, R.D., Searle, M.P., Simpson, R.L., 2004. Strain, deformation temperatures and vorticity of flow at the top of the Greater Himalayan Slab, Everest Massif, Tibet. *Journal of the Geological Society (London)* 161, 305–320.
- Leitner, B., Eberhart-Phillips, D., Anderson, H., Nabelek, J.L., 2001. A focussed look at the Alpine Fault, New Zealand: Seismicity, focal mechanisms, and stress observations. *Journal of Geophysical Research* 106 (B2), 2193–2220.
- Lister, G.S., 1977. Discussion: Crossed girdle c-axis fabrics in quartzites plastically deformed by plane strain and progressive simple shear. *Tectonophysics* 39, 51–54.
- Lister, G.S., Hobbs, B.E., 1980. The simulation of fabric development during plastic deformation and its application to quartzite: the influence of deformation history. *Journal of Structural Geology* 2, 335–352.
- Lister, G.S., Paterson, M.S., 1979. The simulation of fabric development during plastic deformation and its application to quartzite: fabric transitions. *Journal of Structural Geology* 1 (2), 99–115.
- Lister, G.S., Price, G.P., 1978. Fabric development in a quartz-feldspar mylonite. *Tectonophysics* 49 (1–2), 37–78.
- Lister, G.S., Snoke, A.W., 1984. S–C Mylonites. *Journal of Structural Geology* 6 (6), 617–638.
- Lister, G.S., Patterson, M.S., Hobbs, B.E., 1978. The simulation of fabric development in plastic deformation and its application to quartzite; the model. *Tectonophysics* 45 (2–3), 107–158.
- Little, T.A., Holcombe, R.J., Ilg, B.R., 2002a. Ductile fabrics in the zone of active oblique convergence near the Alpine Fault, New Zealand: identifying the neotectonic overprint. *Journal of Structural Geology* 24, 193–217.
- Little, T.A., Holcombe, R.J., Ilg, B.R., 2002b. Kinematics of oblique collision and ramping inferred from microstructures and strain in middle crustal rocks, central Southern Alps, New Zealand. *Journal of Structural Geology* 24, 219–239.
- Little, T.A., Cox, S., Vry, J.K., Batt, G., 2005. Variations in exhumation level and uplift rate along the oblique-slip Alpine Fault, central Southern Alps, New Zealand. *Geological Society of America Bulletin* 117 (5/6), 707–723.
- Mainprice, D., Bouches, J.-L., Blumenfeld, P., 1986. Dominant c slip in naturally deformed quartz: Implications for dramatic plastic softening at high temperature. *Geology* 14, 819–822.
- Molnar, P., Anderson, H.J., Audoin, E., Eberhardt-Phillips, D., Gledhill, K.R., Klosko, E.K., McEvilly, T.V., Okaya, D., Savage, M.K., Stern, T., Wu, F.T., 1999. Continuous deformation versus faulting through the continental lithosphere: tests using New Zealand as a laboratory for the study of continental dynamics. *Science* 286, 516–519.
- Norris, R.J., Cooper, A.F., 1995. Origin of small-scale segmentation and transpressional thrusting along the Alpine Fault, New Zealand. *Geological Society of New Zealand Bulletin* 107, 231–240.
- Norris, R.J., Cooper, A.F., 1997. Erosional control on the structural evolution of a transpressional thrust complex on the Alpine Fault, New Zealand. *Journal of Structural Geology* 19 (10), 1323–1343.
- Norris, R.J., Cooper, A.F., 2001. Late Quaternary slip rates and slip-partitioning on the Alpine Fault, New Zealand. *Journal of Structural Geology* 23, 507–520.
- Norris, R.J., Cooper, A.F., 2003. Very high strains recorded in mylonites along the Alpine Fault, New Zealand: implications for the deep structure of plate boundary faults. *Journal of Structural Geology* 25, 2141–2157.
- Nye, J., 1953. The flow law of ice from measurements in glacier tunnels, laboratory experiments and the Jungfraufim borehole experiment. *Proceedings of the Royal Society, London* 219, 477–489.
- Okudaira, T., Takeshita, T., Hara, I., Ando, J., 1995. A new estimate of the conditions for transition from basal to prism [c] slip in naturally deformed quartz. *Tectonophysics* 250 (1–3), 31–46.
- Passchier, C.W., Trouw, R.A.J., 1996. *Micro-Tectonics*. Springer, Berlin Heidelberg.
- Pfiffner, O.A., Ramsay, J.G., 1982. Constraints on geological strain rates; arguments from finite strain states of naturally deformed rocks. *Journal of Geophysical Research* B87 (1), 311–321.
- Poirier, J.P., 1980. Shear localisation and shear instability in materials in the ductile field. *Journal of Structural Geology* 2 (1/2), 135–142.
- Price, G.P., 1985. Preferred orientations in quartzites. In: Wenk, H.-R. (Ed.), *Preferred Orientations in Deformed Metals and Rocks: an introduction to modern texture analysis*. Academic Press, Orlando, FL, pp. 385–406.
- Prior, D.J., 1988. Deformation processes in the Alpine Fault Mylonites, South Island, New Zealand. PhD thesis, University of Leeds.
- Prior, D.J., 1993. Sub-critical fracture and associated retrogression of garnet during mylonitic deformation. *Contributions to Mineralogy and Petrology* 113, 545–556.
- Prior, D.J., Knipe, R.J., Handy, M.R., 1990. Estimates of rates of microstructural changes in mylonites. In: Knipe, R.J., Rutter, E.H. (Eds.), *Deformation Mechanisms, Rheology and Tectonics*. Geological Society Special Publications, 54. The Geological Society, London, pp. 309–320.
- Prior, D.J., Boyle, A.P., Brenker, F., Cheadle, M.C., Day, A., Lopez, G., Purezzo, L., Potts, G.J., Reddy, S., Spiess, R., Timms, N.E., Trimby, P.W., Wheeler, J., Zetterstrom, L., 1999. The application of electron backscatter diffraction and orientation contrast imaging in the SEM to textural problems in rocks. *American Mineralogist* 84, 1741–1759.
- Ralser, S., Hobbs, B.E., Ord, A., 1991. Experimental deformation of a quartz mylonite. *Journal of Structural Geology* 13 (7), 837–850.
- Ramsay, J.G., Huber, M.I., 1983. *The Techniques of Modern Structural Geology, Volume 1: Strain Analysis*. Academic Press, New York.
- Read, S.E., 1994. Alpine Fault segmentation and range front structure between Gaunt Creek and Little Man River, near Whataroa, central Westland, New Zealand. BSc(Hons) thesis, University of Otago.
- Schmid, S.M., Casey, M., 1986. Complete fabric analysis of some commonly observed quartz c-axis patterns. In: Hobbs, B.E., Heard, H.C. (Eds.), *Mineral and Rock Deformation: Laboratory Studies—The Paterson Volume*. American Geophysical Union Monograph, 36. American Geophysical Union, pp. 246–261.
- Sibson, R.H., 1974. Frictional constraints on thrust, wrench and normal faults. *Nature* 249, 542–545.
- Sibson, R.H., 1977. Fault rocks and fault mechanisms. *Journal of the Geological Society, London* 133, 191–213.

- Sibson, R.H., 1998. Brittle failure mode plots for compressional and extensional tectonic regimes. *Journal of Structural Geology* 20 (5), 655–660.
- Sibson, R.H., White, S.H., Atkinson, B.K., 1979. Fault rock distribution and structure within the Alpine Fault zone: a preliminary account. *Royal Society of New Zealand Bulletin* 18, 55–65.
- Simpson, C., 1980. Oblique girdle orientation patterns of quartz c-axes from a shear zone in the basement core of the Maggia nappe, Ticino, Switzerland. *Journal of Structural Geology* 2 (1–2), 234–247.
- Stipp, M., Steunitz, H., Heilbronner, R., Schmid, S.M., 2002a. Dynamic recrystallisation of quartz: correlation between natural and experimental conditions. In: De Meer, S., Drury, M.R., De Bresser, J.H.P., Pennock, G.M. (Eds.), *Deformation Mechanisms, Rheology and Tectonics: Current Status and Future Perspectives*. Geological Society Special Publications, 200. The Geological Society, London, pp. 171–190.
- Stipp, M., Steunitz, H., Heilbronner, R., Schmid, S.M., 2002b. The eastern Tonale fault zone: a ‘natural laboratory’ for crystal plastic deformation of quartz over a temperature range from 250 to 700°C. *Journal of Structural Geology* 24, 1861–1884.
- Sutherland, R., 1995. The Australia-Pacific boundary and Cenozoic plate motions in the SW Pacific: Some constraints from Geosat data. *Tectonics* 14 (4), 819–831.
- Sutherland, R., Berryman, K.R., Norris, R.J., 2007. Quaternary slip rate and geomorphology of the Alpine Fault: implications for kinematics and seismic hazard in southwest New Zealand. *Geological Society of America Bulletin* 118, 464–474.
- Takeshita, T., 1996. Estimate of physical conditions for deformation based on c-axis transitions in naturally deformed quartzite. *Journal of the Geological Society of Japan* 102 (3), 211–222.
- ten Grotenhuis, S.M., Trow, R.A.J., Passchier, C.W., 2003. Evolution of mica fish in mylonitic rocks. *Tectonophysics* 372, 1–21.
- Tippett, J.M., Kamp, P.J.J., 1993. Fission track analysis of the Late Cenozoic vertical kinematics of continental Pacific Crust, South Island, New Zealand. *Journal of Geophysical Research* B9, 16,119–16,148.
- van Daalen, M., Heilbronner, R., Kunze, K., 1999. Orientation analysis of localized shear deformation in quartz fibers at the brittle-ductile transition. *Tectonophysics* 303, 83–107.
- Vry, J.K., Baker, J., Maas, R., Little, T.A., Grapes, R., Dixon, M., 2004. Zoned (Cretaceous and Cenozoic) garnet and timing of high grade metamorphism, Southern Alps, New Zealand. *Journal of Metamorphic Geology* 22, 137–157.
- Wagner, W., Overhoff, U., 2006. *ThermoFluids*. Springer, Berlin Heidelberg.
- Wagner, W., Prub, A., 2002. The IAPWS formulation 1995 for the thermodynamic properties of ordinary water substance for general and scientific use. *Journal of Physical and Chemical Reference Data* 31 (2), 387–535.
- Walcott, R.I., 1998. Modes of oblique compression: Late Cenozoic tectonics of the South Island, New Zealand. *Reviews of Geophysics* 36 (1), 1–26.
- Wenk, H.-R., 1998. Deformation of mylonite in Palm Canyon, California, based on xenolith geometry. *Journal of Structural Geology* 20 (5), 559–571.
- Wenk, H.-R., Christie, J.M., 1991. Comments on the interpretation of deformation textures in rocks. *Journal of Structural Geology* 13 (10), 1091–1110.
- White, S.H., 1976. The effects of strain on microstructures, fabrics, and deformation mechanisms in quartzites. *Philosophical Transactions of the Royal Society of London* A283, 69–86.
- Willingshofer, E., Neubauer, F., 2002. Structural evolution of an antiformal window: the Scheiblingkirchen Window (Eastern Alps, Austria). *Journal of Structural Geology* 24, 1603–1618.